JOURNAL OF PETROLOGY | VOLUME 47 | NUMBER 7 | PAGES 1439–1465 | 2006 | doi:10.1093/petrology/egl018

Comparison of ^{40}Ar–^{39}Ar and Rb–Sr Data on Phengites from the UHP Brossasco–Isasca Unit (Dora Maira Massif, Italy): Implications for Dating White Mica

GIANFRANCO DI VINCENZO[1]*, SONIA TONARINI[1], BRUNO LOMBARDO[2], DANIELE CASTELLI[2,3] AND LUISA OTTOLINI[4]

[1]ISTITUTO DI GEOSCIENZE E GEORISORSE–CNR, VIA MORUZZI 1, I-56124 PISA, ITALY

[2]ISTITUTO DI GEOSCIENZE E GEORISORSE–CNR, SEZIONE DI TORINO, VIA VALPERGA CALUSO 35, I-10125 TORINO, ITALY

[3]DIPARTIMENTO DI SCIENZE MINERALOGICHE E PETROLOGICHE, VIA VALPERGA CALUSO 35, I-10125 TORINO, ITALY

[4]ISTITUTO DI GEOSCIENZE E GEORISORSE–CNR, SEZIONE DI PAVIA, VIA FERRATA 1, I-27100 PAVIA, ITALY

RECEIVED JULY 31, 2005; ACCEPTED MARCH 7, 2006; ADVANCE ACCESS PUBLICATION MARCH 30, 2006

Different lithologies (impure marble, eclogite and granitic orthogneiss) sampled from a restricted area of the coesite-bearing Brossasco–Isasca Unit (Dora Maira Massif) have been investigated to examine the behaviour of ^{40}Ar–^{39}Ar and Rb–Sr systems in phengites developed under ultrahigh-pressure (UHP) metamorphism. Mineralogical and petrological data indicate that zoned phengites record distinct segments of the P–T *path: prograde, peak to early retrograde in the marble, peak to early retrograde in the eclogite, and late retrograde in the orthogneiss. Besides major element zoning, ion microprobe analysis of phengite in the marble also reveals a pronounced zoning of trace elements (including Rb and Sr). ^{40}Ar–^{39}Ar apparent ages (~35–62 Ma, marble; ~89–170 Ma, eclogite; ~35–52 Ma, orthogneiss), determined through Ar laser-probe data on phengites (step-heating and* in situ *techniques), show wide intra-sample and inter-sample variations closely linked to within-sample microchemical variations: apparent ages decrease with decreasing celadonite contents. These data confirm previous reports on excess Ar and, more significantly, highlight that phengite acted as a closed system in the different lithologies and that chemical exchange, not volume diffusion, was the main factor controlling the rate of Ar transport. Conversely, a Rb–Sr internal isochron from the same eclogite yields an age of ~36 Ma, overlapping with the time of the UHP metamorphic peak determined through U–Pb data and thereby corroborating the previous conclusion that UHP metamorphism and early retrogression occurred in close succession. Different phengite fractions of the marble yield calcite–phengite isochron ages of ~36 to ~60 Ma. Although this time interval matches Ar ages from the same sample, Rb–Sr data from phengite are not entirely consistent with the whole dataset. According to trace element variations in phengite, only Rb–Sr data from two wet-ground phengite separates, yielding ages of ~36 and ~41 Ma, are internally consistent. The oldest age obtained from a millimetre-sized grain fraction enriched in prograde–peak phengites may represent a minimum age estimate for the prograde phengite relics. Results highlight the potential of the* in situ *^{40}Ar–^{39}Ar laser technique in resolving discrete* P–T *stages experienced by eclogite-facies rocks (provided that excess Ar is demonstrably a negligible factor), and confirm the potential of Rb–Sr internal mineral isochrons in providing precise crystallization ages for eclogite-facies mineral assemblages.*

KEY WORDS: *^{40}Ar–^{39}Ar dating; Rb–Sr dating; phengite; SIMS; UHP metamorphism*

*Corresponding author. Fax: +39 050 3152360. E-mail: g.divincenzo@igg.cnr.it

INTRODUCTION

Dating eclogite-facies rocks and their subsequent retrogression at upper crustal levels represents an invaluable, essential tool for constraining the rate of exhumation of these rocks from mantle depths, thus allowing development of theoretical models. To temporally quantify geological processes, isotopic ages must be linked to a specific stage of the *P–T*–deformation evolution of a rock. In the most popular approach, this link is established using the closure temperature concept (T_c; Dodson, 1973). When interpreting isotopic ages in terms of temperature only, this concept has been used to derive the temperature–time path by analysing minerals with different T_c. However, high-pressure (HP) and ultrahigh-pressure (UHP) metamorphic rocks are peculiar systems, which experienced extreme physical conditions characterized by limited aqueous fluids with restricted mobility, and consequently by limited mass transfer and exceedingly sluggish reaction kinetics. In these circumstances, one cannot assume that radiogenic daughters diffusing out of a mineral are efficiently removed at the grain boundary and that the concentration of that isotope at the grain boundary is zero. In addition, in UHP–HP terrains, limited fluid availability and strain partitioning may determine the persistence through the whole metamorphic cycle of relic minerals and/or mineral assemblages from precursor metamorphic or igneous rocks and/or pertaining to different stages of the UHP–HP tectonometamorphic evolution, including the prograde (subduction) and retrograde (exhumation) path. Complications in the application of the closure temperature concept to natural samples thus arise from mineral complexities (i.e. coexistence of multiple and diachronous mineral generations), which produce spatially and temporally inhomogeneous mineral structures. Numerous studies have directly or indirectly shown that the mobility of incompatible trace elements (including doubly charged Sr and unbound neutral Ar) within a mineral phase seems to be strictly coupled with that of structure-forming major elements, sustaining the hypothesis that mineral relics carry isotope inheritance (e.g. Verschure *et al.*, 1980; Hammerschmidt & Frank, 1991; Hames & Cheney, 1997; Villa, 1998; Kühn *et al.*, 2000; Villa *et al.*, 2000; Di Vincenzo *et al.*, 2001, 2004; Glodny *et al.*, 2002, 2003). This hypothesis requires careful evaluation at the micrometre and possibly the sub-micrometre scale of the mineral (in)homogeneity, and suggests that geochronological investigations that use a bulk approach are prone to yield geologically meaningless ages by averaging diachronous mineral generations with potentially distinct isotope records.

In situ U–Pb dating of accessory minerals by SHRIMP (sensitive high-resolution ion microprobe) has great potential in dating different *P–T* stages of metamorphic rocks. This is due to the very compact structure of accessory minerals with high U/Pb ratios, which inhibits the kinetics of diffusion and recrystallization (e.g. Dahl, 1997). Although cathodoluminescence and X-ray imaging coupled with detailed microtextural and microchemical characterization (including trace element geochemistry) represents a definite advantage in interpreting the various growth zones (e.g. Rubatto & Gebauer, 2000), the link between different spot ages and specific physical conditions may be problematic (e.g. Hacker *et al.*, 1998; Gray *et al.*, 2004) and not as direct as that established for isotopic ages obtained from phases that are part of the mineral assemblage used to derive *P–T* paths. To overcome these drawbacks, different major and minor phases (e.g. garnet, rutile, epidote, titanite, staurolite) have been used in U–Pb dating studies. The low U/Pb and Th/Pb ratios, however, make these phases strongly sensitive to the isotopic composition used to correct the initial Pb contribution (see, e.g. Romer, 2001) and their apparent ages may be strongly influenced by the presence of mineral inclusions with high U/Pb and Th/Pb ratios (e.g. Dahl & Frei, 1998).

Of the major minerals, potassic white mica is, in principle, ideal for linking isotopic ages to a specific *P–T*–deformation stage: it is commonly part of the mineral assemblage used to define *P–T* conditions, and its fabric provides an important means to establish the temporal relationship between deformation and physical conditions. In addition, the favourable Rb/Sr ratio makes potassic white mica well suited to dating by the Rb–Sr internal mineral isochron approach, and the high K content allows the application of the ^{40}Ar–^{39}Ar laser extraction technique for *in situ* dating at a high spatial resolution, with potential to directly link textural–chemical information to Ar age records. However, on the one hand a Rb–Sr internal mineral isochron (commonly based on bulk samples) should be strictly derived from equilibrium mineral assemblages belonging to a specific segment of the *P–T* path (Glodny *et al.*, 2002, 2003, 2005), avoiding relict and retrograde minerals. On the other hand, a common drawback when using white mica for ^{40}Ar–^{39}Ar geochronological investigation in HP and UHP terrains is that Ar apparent ages can be significantly older than those obtained from the same rock sample using different radioisotopic systems (e.g. Tonarini *et al.*, 1993; Li *et al.*, 1994; Ruffet *et al.*, 1997; Sherlock *et al.*, 1999). In many natural examples this phenomenon has been attributed to the presence of parentless ^{40}Ar (i.e. excess Ar), but only rarely are the meaning and origin of excess Ar and the role of inherited Ar adequately discussed. Furthermore, when comparing ^{40}Ar–^{39}Ar data with Rb–Sr results from white mica, the possible presence of parent–daughter zoning within the mineral grain is commonly not investigated and the possible consequences are ignored.

We address these issues by studying phengites from different lithologies of the UHP Brossasco–Isasca Unit (BIU) in the Dora Maira Massif (western Alps). The rationale for the present study stems from the discovery by Ferraris *et al.* (2005) of a strong structural complexity at the sub-microscopic scale in phengite cores from an impure UHP marble of the BIU. Those workers showed that complex nanostructures formed by coexisting diachronous phengite domains a few tens of nanometres wide and characterized by different celadonite contents cannot be revealed by routine mineral investigation at the microscopic scale [i.e. using the scanning electron microscope equipped with an energy dispersive system (SEM–EDS) and the electron microprobe (EMP)]. More significantly, phengite in this marble preserves a nearly continuous record of the whole *P–T* path experienced by the BIU during the Alpine cycle, including relics of the prograde segment. These features, along with the very simple paragenesis and the well-defined *P–T*–time path recently reconstructed for the BIU (Rubatto & Hermann, 2001), make this impure marble an excellent specimen for investigating the effects of mineralogical complexity on isotopic dating of UHP white micas. In the present study we fully exploited the potential of the ^{40}Ar–^{39}Ar method, using both laser step-heating and laser *in situ* techniques in conjunction with textural and chemical characterization at the microscale. ^{40}Ar–^{39}Ar data were compared with Rb–Sr ages from the same sample, and with data obtained from a well-preserved eclogite and two granitic orthogneisses collected from the same metamorphic unit.

GEOLOGICAL BACKGROUND

The Dora Maira Massif, Monte Rosa and Gran Paradiso represent the Internal Crystalline Massifs of the Penninic Zone of the western Alps (Fig. 1). These massifs are interpreted as slices of the palaeo-European margin exhumed after attempted subduction and Alpine continent–continent collision. They mostly derived from a Variscan (350–300 Ma) amphibolite-facies metamorphic basement, which was variably intruded by late-orogenic granitoids (310–275 Ma). Country metamorphic rocks and granitoids metamorphosed during the Alpine cycle are referred to as polymetamorphic and monometamorphic complexes, respectively (Compagnoni *et al.*, 1995). In the southern part of the Dora Maira Massif, Chopin *et al.* (1991) distinguished several crustal slices that recorded different *P–T* metamorphic conditions during the Alpine cycle, ranging from epidote-blueschist-, to quartz-eclogite- and coesite-eclogite-facies conditions. In the coesite-bearing BIU, the polymetamorphic complex consists of phengite–garnet–kyanite ± jadeite paraschists, and decimetre- to decametre-thick lenses of eclogite and marble (Fig. 1). The monometamorphic complex is composed of albite orthogneisses, locally with augen structure, which contain the well-known coesite-bearing pyrope whiteschists (Chopin, 1984). More details on the regional geology, petrographic descriptions of the various lithologies exposed in the southern Dora Maira Massif, and inferred *P–T* paths can be found in numerous studies (e.g. Chopin, 1984; Biino & Compagnoni, 1991; Chopin *et al.*, 1991; Kienast *et al.*, 1991; Schertl *et al.*, 1991; Sharp *et al.*, 1993; Compagnoni *et al.*, 1995; Chopin & Schertl, 1999; Nowlan *et al.*, 2000; Compagnoni & Hirajima, 2001). As for peak *P–T* conditions, there is excellent agreement among temperature estimates obtained using different approaches on various lithologies. Numerous studies report comparable peak temperatures of 700–750°C (Chopin *et al.*, 1991; Kienast *et al.*, 1991; Sharp *et al.*, 1993; Nowlan *et al.*, 2000). In contrast, there is less agreement on peak pressures. Apart from the occurrence of coesite, suggesting at least ~2·7 GPa at 700°C, pressure estimates are mainly in the range of 3·0–3·7 GPa (Schertl *et al.*, 1991; Compagnoni *et al.*, 1995; Nowlan *et al.*, 2000). Hermann (2003), by comparing phase relations and phase compositions in the pyrope whiteschist with experimental data, inferred a peak pressure of 4·3 ± 0·3 GPa, thus suggesting that the coesite-bearing BIU reached diamond-facies metamorphic conditions. Further evidence for peak metamorphic conditions within the diamond stability field has been recently reported for impure marbles by Castelli *et al.* (2004). Petrological details on this rock type are reported in the next section.

Previous geochronology

The UHP metamorphism of the BIU was long believed to be Cretaceous in age. This inference was based on conventional U–Pb zircon data from the pyrope whiteschist (Paquette *et al.*, 1989), which yielded a lower intercept age of 121+12/–29 Ma in a concordia diagram. This age was found to be in agreement with a Rb–Sr white mica–whole-rock age of 96 ± 4 Ma (Paquette *et al.*, 1989), and with an ^{40}Ar–^{39}Ar plateau age of ~105 Ma obtained by Monié & Chopin (1991) on white mica separated from the same rock type. In contrast, Tilton *et al.* (1989, 1991) proposed a rather different scenario in which the pyrope crystals of the UHP whiteschists grew at 38–40 Ma. This interpretation was based on: conventional U–Pb zircon data, yielding in a concordia diagram a lower intercept age of 38·0 ± 2·8 (2σ) Ma; Sm–Nd garnet results from seven samples, yielding an errorchron with an apparent age of 38·3 ± 4·5 (2σ); and U–Pb data on pyrope, ellenbergerite, monazite and white micas, giving apparent U–Pb and Th–Pb ages of ~31 to ~35 Ma. The Cretaceous age for Alpine metamorphism

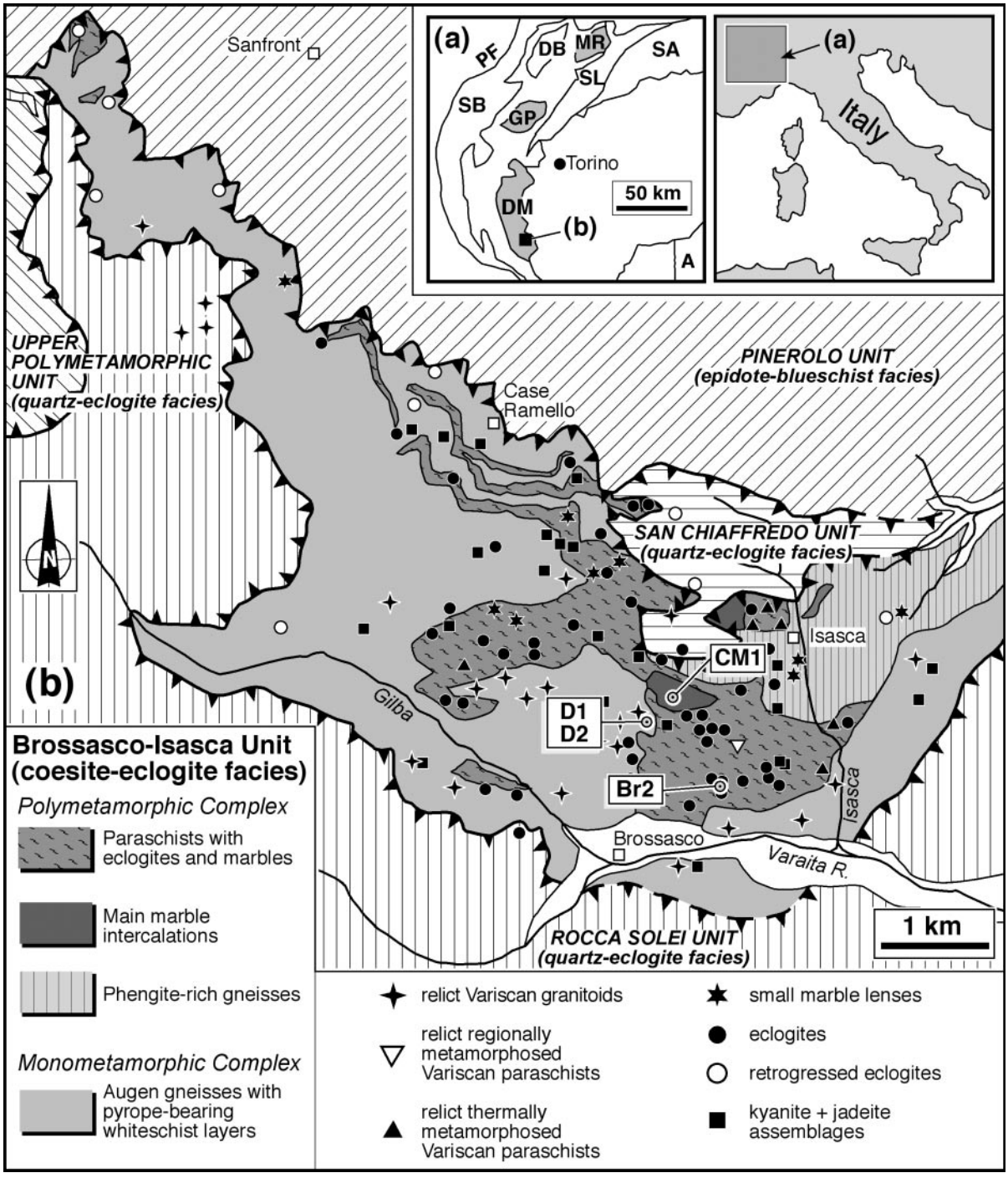

Fig. 1. Simplified geological map of the coesite-bearing 'Brossasco–Isasca Unit' (modified after Compagnoni & Rolfo, 2003) and sample location. The inset (a) shows a tectonic sketch map of the western Alps. Internal Crystalline Massifs (grey fields): MR, Monte Rosa; GP, Gran Paradiso; DM, Dora Maira. SB, Grand St. Bernard Zone; DB, Dent Blanche nappe; SL, Sesia Lanzo Zone; SA, Southern Alps; PF, Penninic frontal thrust; A, Apennines.

was also questioned by Arnaud & Kelley (1995): using the laser ablation ^{40}Ar–^{39}Ar technique to study the statically recrystallized Brossasco metagranite, they found minerals contaminated by excess Ar. The Tertiary age for the UHP stage in the BIU was confirmed by Gebauer *et al.* (1997) and by Duchêne *et al.* (1997). The latter study reported a Lu–Hf age of 32·8 ± 1·2 Ma, which was obtained on a garnet–whole-rock pair from a pyrope

whiteschist. In the former study, U–Pb SHRIMP data on zircons from different rock types in a UHP whiteschist lens consistently showed domains with an average age of 35·4 ± 1·0 Ma, interpreted as the time of UHP metamorphic peak. Gebauer *et al.* (1997) also reported fission-track data on zircon with a weighted mean age of 29·9 ± 2·7 Ma. The *P*–*T*–time path of the BIU was more recently refined by Rubatto & Hermann (2001), who used SHRIMP for *in situ* dating of single growth zones of titanite grains from two calc-silicate nodules in marbles. Titanite domains thought to have developed during the UHP stage yielded, in agreement with the results of Gebauer *et al.* (1997), a mean age of 35·1 ± 0·9 Ma, those developed during exhumation at ~35 km a mean age of 32·9 ± 0·9 Ma, and those crystallized at ~17 km a mean age of 31·8 ± 0·5 Ma. These data, along with the fission-track data of Gebauer *et al.* (1997), allowed the reconstruction of one of the best-documented exhumation paths for UHP terrains. This *P*–*T*–*t* path will be used as a temporal frame of reference in the present study.

As for the ^{40}Ar–^{39}Ar dating method, phengites from the BIU and from the overlying HP unit of the central Dora Maira have been analysed by different extraction techniques, including furnace step-heating analysis of bulk samples, laser step-heating of single grains and *in situ* analysis of single grains and on rock chips (Scaillet *et al.*, 1990, 1992; Monié & Chopin, 1991; Hammerschmidt *et al.*, 1995; Scaillet, 1996; Monié & Bosch, 2000). Nevertheless, the inter-grain and intra-grain distribution of Ar ages in white mica has so far been documented in detail in the HP units of the central Dora Maira only (Scaillet *et al.*, 1990, 1992; Scaillet, 1996), but not in rocks of the BIU. ^{40}Ar–^{39}Ar apparent ages range widely (Fig. 2), from ~35–40 Ma to ~300 Ma, and mainly fall in the 35–40 to 150 Ma time interval. Ar apparent ages, therefore, range from the time of the inferred UHP metamorphism to ages that compare with those of the Variscan protoliths. Furthermore, Hammerschmidt *et al.* (1995) reported unrealistically old incremental ^{40}Ar–^{39}Ar ages of up to 1 Ga for phlogopite pseudomorphing garnet in a pyrope whiteschist, and Arnaud & Kelley (1995) obtained *in situ* ^{40}Ar–^{39}Ar apparent ages of 565 and 614 Ma for phengite cores from the undeformed Brossasco metagranite. If on the one hand these data unequivocally indicate that phengites from Dora Maira are heavily, but variably, contaminated by excess Ar, in most cases yielding obviously meaningless old ages, on the other hand published data indicate the existence of a strong lithological and petrological control on the extent of excess Ar contamination. Figure 2 shows that orthogneisses yield the youngest apparent ages and eclogites the oldest, whereas apparent ages from HP metapelites and UHP–HP whiteschists tend to fall between these. Moreover, samples characterized by a more advanced retrogression at upper crustal levels exhibit white micas with comparatively lower celadonitic contents and younger Ar apparent ages (Fig. 2).

As for the Rb–Sr systematics, data on white micas from the BIU are scarce. Apart from the ~96 Ma apparent age cited above (Paquette *et al.*, 1989), Tilton *et al.* (1989, 1991) reported Rb–Sr data that failed to produce reliable trends. More recently, Monié & Bosch (2000) reported a Rb–Sr age of ~38 Ma for phengite from an UHP eclogite.

SAMPLE DESCRIPTION AND PETROLOGICAL DATA

Sample CM1—phengite marble

Sample CM1 comes from the hand specimen investigated by Ferraris *et al.* (2005) and was collected in the Costa Monforte marble lens (Fig. 1), a body of ~800 m length and a few tens of metres thickness, enclosed in metasedimentary schists. The Costa Monforte marble is generally medium grained and is locally transected by decimetre-thick fine-grained shear zones. It shows a wide range of fabrics, from coarse-grained granoblastic polygonal through mortar, to very fine-grained mylonitic, and includes both calcite- and dolomite-rich varieties. Additional minerals with highly variable abundances are phengite, quartz, garnet, Na-rich clinopyroxenes, epidotes, feldspars, Ca-amphiboles, chlorite and biotite. Accessory minerals include zircon, titanite and rutile. Carbonate crystals may be either equant or elongated, with a preferred dimensional orientation parallel to that defined by the scattered silicate aggregates. Castelli *et al.* (2004), studying a dolomite-poor marble with the assemblage calcite + clinopyroxene + garnet ± phengite ± rutile, obtained peak conditions of 720–730°C and 3·9 ± 0·1 GPa, in agreement with the results of Hermann (2003). The studied sample is medium to fine grained, with millimetre-thick layers rich in phengite and with rare epidote aggregates. Phengite crystals are a few hundred micrometres to ~1·5 mm long and are locally rimmed by K-feldspar. Spot analyses reveal that the celadonite content is highly variable at the single grain scale. Si atoms per formula unit (a.p.f.u.) range from 3·57 to 3·21 (Table 1) from the core to the rim; the data define a nearly continuous variation as shown in Fig. 3. X-ray maps for Al in five phengite flakes from the >0·50 mm grain fraction (Fig. 4), in agreement with observations of Ferraris *et al.* (2005), indicate that the larger grains consist of: (1) a core area with high Si contents of 3·54–3·45 a.p.f.u.; (2) a mantle area with Si contents ranging from ~3·3 to ~3·4 a.p.f.u.; (3) locally, a very thin and discontinuous rim with a Si content of ~3·2 a.p.f.u. Smaller flakes generally have lower celadonite contents than the core areas of the larger grains. More significantly,

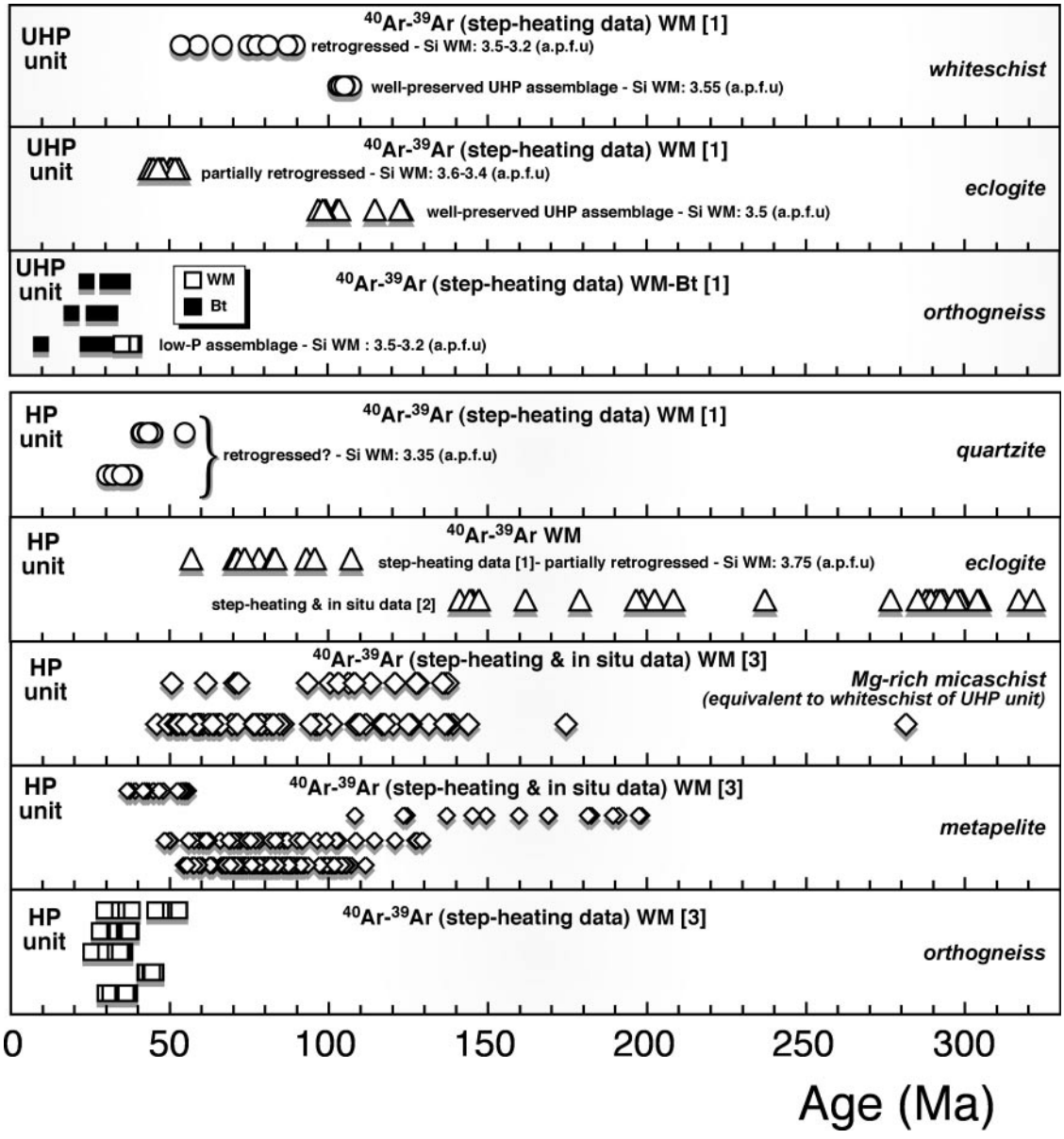

Fig. 2. Published ^{40}Ar–^{39}Ar ages in white mica (WM) and biotite (Bt) from different lithologies of the UHP (BIU) and HP units of the Dora Maira Massif. Each symbol refers to ages from *in situ* analysis or individual steps, with more than 1% of the total $^{39}Ar_K$ released, from incremental heating analysis. Data on the same line are from a single sample. References: [1] Monié & Chopin (1991); [2] Scaillet (1996); [3] Scaillet *et al.* (1992). Additional Ar data from the BIU are quoted in the text.

Ferraris *et al.* (2005) showed by transmission electron microscopy (TEM) that the core areas have a complex nanostructure made up of two $3T$ polytypes characterized by distinct cell parameters: a phengite with a lower Si content [3·38 a.p.f.u.—Phe (a)] and another with a higher Si content [3·61 a.p.f.u.—Phe (b)]. In contrast, the mantle overgrowths consist of only one type of $3T$ phengite with a Si content that decreases continuously toward the rim of crystals (from 3·41 to 3·31 a.p.f.u., M1 and M2 mantle, respectively). The discontinuous rim consists of a $2M_1$ polytype. Although the nano-scale features of the core areas did not reveal whether the growth of Phe(a) occurred prior to or after that of Phe(b), Ferraris *et al.* (2005) considered 'Phe(a) earlier than Phe(b)' the most likely interpretation on the basis of available mineral-chemical and microstructural data on phengites from BIU eclogites. They concluded that the complex micro- and nano-scale features of white mica from the Costa Monforte marble arose from the following growth sequence: (1) formation of prograde phengite [Phe(a)]

Table 1: Representative analyses of minerals from the BIU

	Marble CM1 separate grain					Eclogite Br 2 thin section							
	Phe3-1 core	Phe3-2 core	Phe3-3 mantle	Phe3-4 mantle	Phe3-5 rim	Phe1-1 core	Phe1-2 core	Phe1-3 core	Phe1-4 interm.	Phe1-5 interm.	Phe2-1 rim	Phe3-1 core	Phe3-2 interm.
SiO_2	52·77	51·77	51·23	50·33	48·49	54·36	53·10	52·23	51·02	49·92	48·78	54·14	51·01
TiO_2	0·33	0·32	0·32	0·32	0·32		0·56	0·58	0·65	0·85	1·00	0·39	0·64
Al_2O_3	24·49	25·23	26·36	27·60	29·28	22·86	24·30	25·73	27·15	29·09	30·32	22·77	27·10
FeO	1·58	1·80	1·91	1·65	1·86	1·60	1·55	1·72	1·61	1·73	1·72	1·59	2·07
MnO			0·04		0·02						0·04		
MgO	4·71	4·52	4·10	3·67	3·23	5·30	4·52	4·25	3·78	2·78	2·76	5·28	3·87
CaO					0·02								
Na_2O	0·05	0·09	0·06	0·11	0·25		0·39	0·39	0·79	1·16	0·89	0·34	0·49
K_2O	11·65	11·28	11·7	11·59	11·42	11·75	11·19	11·12	10·45	10·03	10·43	11·16	10·81
Total	95·59	95·02	95·75	95·31	94·89	95·88	95·62	96·04	95·44	95·57	95·94	95·67	95·99
	11 oxygens					*11 oxygens*							
Si	3·515	3·470	3·420	3·370	3·269	3·605	3·528	3·459	3·393	3·315	3·238	3·592	3·384
Al	1·922	1·992	2·073	2·178	2·326	1·787	1·903	2·009	2·127	2·276	2·371	1·781	2·119
Ti	0·017	0·016	0·016	0·016	0·016		0·028	0·029	0·032	0·043	0·050	0·019	0·032
Fe^{2+}	0·088	0·101	0·107	0·092	0·105	0·089	0·086	0·095	0·089	0·096	0·095	0·088	0·115
Mn			0·002		0·001						0·002		
Mg	0·467	0·451	0·408	0·366	0·324	0·524	0·447	0·420	0·375	0·275	0·272	0·522	0·383
Ca					0·001								
Na	0·006	0·012	0·008	0·014	0·033		0·051	0·050	0·101	0·149	0·115	0·043	0·064
K	0·990	0·964	0·996	0·990	0·982	0·994	0·948	0·940	0·886	0·849	0·883	0·945	0·915
Total	7·005	7·006	7·029	7·027	7·058	6·998	6·992	7·002	7·005	7·004	7·026	6·993	7·014

	Eclogite Br 2 thin section						Orthogneiss D1 separate grain			thin section	
	Cpx1-1 core	Cpx1-2 rim	Grt1-1 core	Grt2-1 rim	Am1-1 core	Am2-1 rim	Phe1-1 core	Phe1-2 interm.	Phe1-3 rim	Bt1	Bt2
SiO_2	56·73	56·26	38·98	38·97	45·96	47·36	51·78	50·98	50·19	37·92	38·66
TiO_2					0·60	0·53	0·49	0·58	0·81	1·95	1·98
Al_2O_3	11·37	11·23	21·71	21·50	15·19	12·33	24·24	25·07	26·46	16·43	16·11
FeO	3·42	3·54	22·05	23·07	11·74	10·32	6·13	5·96	5·75	22·00	21·14
MnO			0·54	0·54						0·21	0·22
MgO	8·37	8·61	6·33	7·15	11·02	13·16	2·15	2·35	2·35	7·35	7·53
CaO	13·09	13·39	10·76	8·63	8·76	9·92				0·02	0·01
Na_2O	7·24	6·78			4·15	3·42		0·16	0·24	0·24	0·24
K_2O					0·68	0·51	11·60	11·39	11·13	9·90	9·96
Total	100·23	99·81	100·37	99·85	98·09	97·54	96·39	96·49	96·93	96·01	95·84
	4 cations–6 oxygens		*12 oxygens*		*23 oxygens*		*11 oxygens*				
Si	1·999	1·995	2·995	3·005	6·617	6·816	3·497	3·440	3·366	2·899	2·944
Al	0·472	0·470	1·965	1·955	2·577	2·090	1·930	1·993	2·091	1·480	1·446

Table 1: continued

	Eclogite Br 2						Orthogneiss D1				
	thin section						separate grain			thin section	
	Cpx1-1 core	Cpx1-2 rim	Grt1-1 core	Grt2-1 rim	Am1-1 core	Am2-1 rim	Phe1-1 core	Phe1-2 interm.	Phe1-3 rim	Bt1	Bt2
Ti					0·065	0·057	0·033	0·039	0·054	0·112	0·113
Fe^{2+}	0·025	0·006	1·417	1·488	1·413	1·241	0·346	0·336	0·322	1·406	1·346
Fe^{3+}	0·075	0·099									
Mn			0·035	0·035						0·013	0·014
Mg	0·440	0·455	0·725	0·822	2·364	2·822	0·216	0·236	0·234	0·837	0·854
Ca	0·494	0·509	0·886	0·713	1·350	1·529				0·002	0·001
Na	0·495	0·466			1·158	0·955		0·021	0·031	0·035	0·035
K					0·125	0·094	0·999	0·980	0·952	0·966	0·967
Total	4·000	4·000	8·023	8·017	15·670	15·605	7·021	7·045	7·053	7·749	7·721

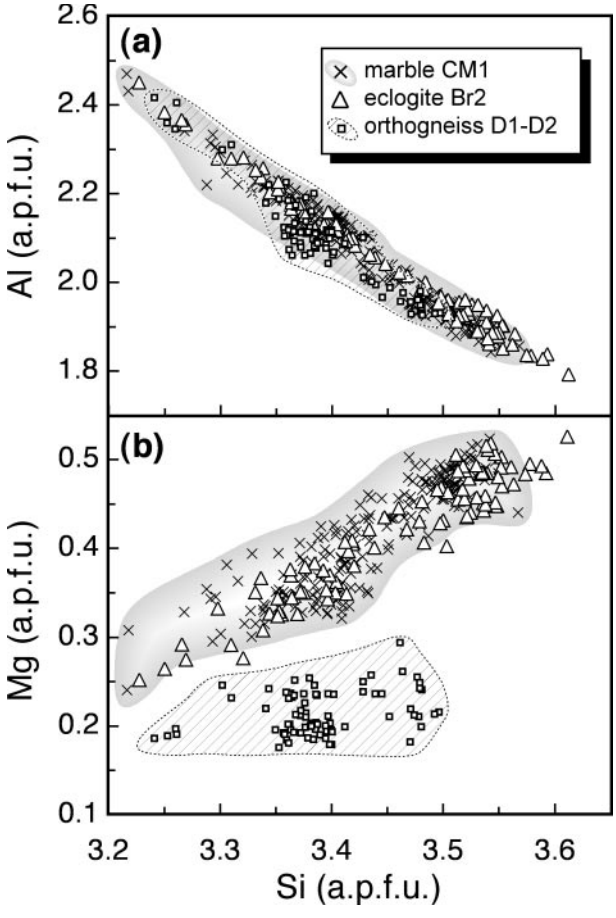

Fig. 3. Compositional range in studied phengites. (a) Al (a.p.f.u.) and (b) Mg (a.p.f.u.) vs Si (a.p.f.u.).

during subduction; (2) partial re-equilibration of Phe(a) under metamorphic peak conditions, and development of nano-scale domains of a higher-Si phengite [Phe(b)]; (3) during exhumation, overgrowth on Phe(a) + Phe(b) cores of phengite characterized by progressively lower Si contents; (4) late growth at upper crustal levels of low-celadonite rims. The prograde, peak and retrograde growth stages of phengite in the Costa Monforte Marble are schematically illustrated in Fig. 5 and qualitatively plotted on the *P–T* path reconstructed for the BIU by Compagnoni *et al.* (1995), modified on the basis of peak conditions estimated by Castelli *et al.* (2004).

In Fig. 4, spot data from five phengite grains are compared with those obtained from different flakes of the 0·16–0·25 mm fraction and from phengites analysed in thin sections. It should be noted that, taking into account the maximum celadonite content in phengite mantle M1 of Ferraris *et al.* (2005), phengite compositions with a Si content significantly higher than 3·41 a.p.f.u. should correspond to mixtures of prograde and peak phengite, with the latter becoming proportionally more important than the former as the celadonite content increases. X-ray maps and Si content frequency (Fig. 4) indicate that proportions of core and mantle phengite can vary greatly from grain to grain, and most probably even between the two grain fractions. Larger grains (i.e. 1, 2, 3; Fig. 4) are enriched in core domains relative to the smaller grains (i.e. 5, Fig. 4) and to the 0·16–0·25 mm grain fraction, which seem to be enriched in mantle phengites instead.

Figure 6 displays the variation of some major and trace elements along two core–rim traverses in grain (3) of Fig. 4. Moving from the core to the rim, the Sr content

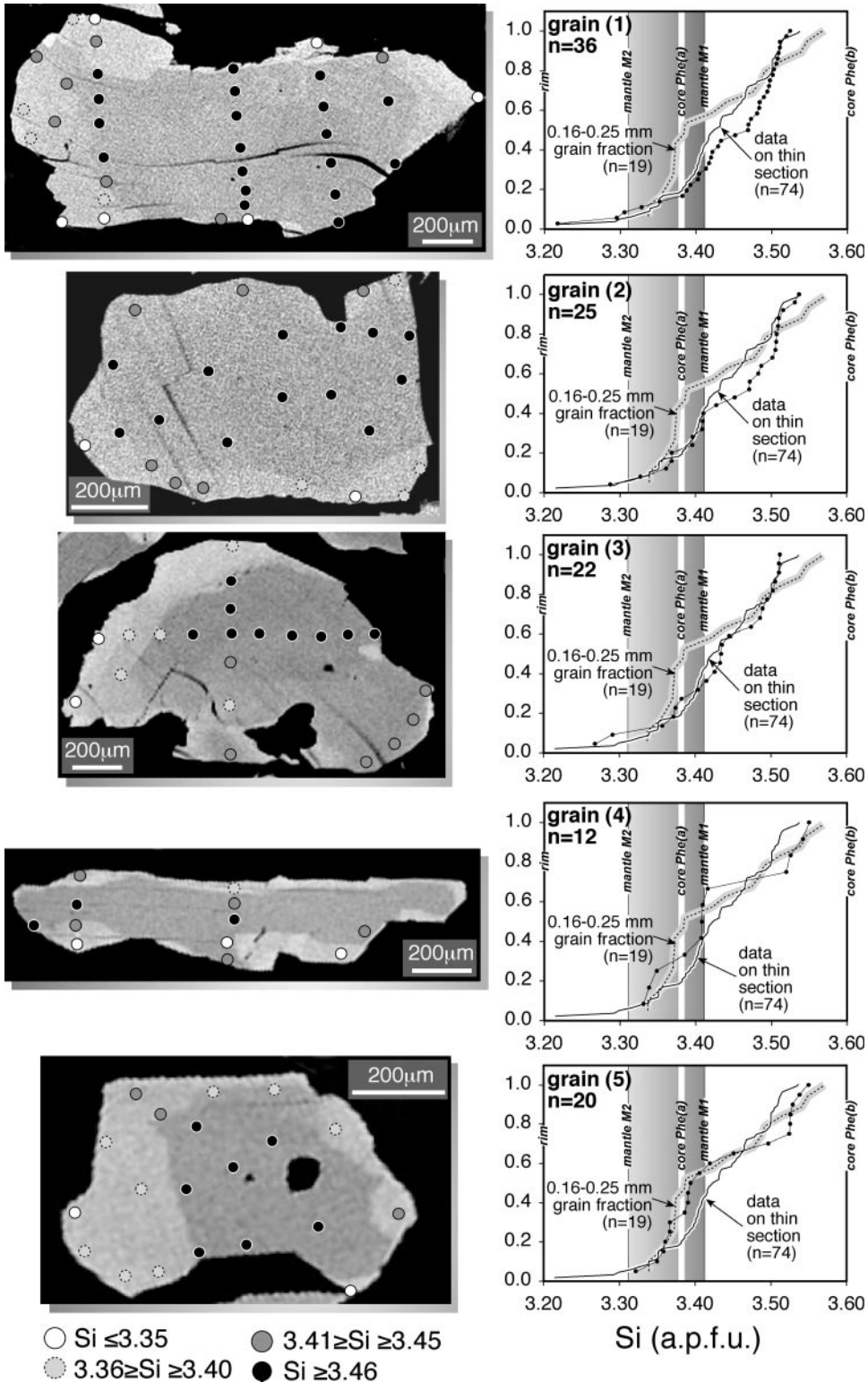

Fig. 4. X-ray maps of Al acquired with an SEM-EDS system of five phengite flakes recovered from the >0·50 mm grain fraction of marble CM1. Locations of SEM-EDS spot analyses are also shown, with different symbols corresponding to various ranges of Si (a.p.f.u.) contents. On the right, frequency diagram of Si (a.p.f.u.) contents in each flake from spot analyses (dots) compared with those obtained from different phengite grains of the 0·16–0·25 mm grain fraction and in thin section. The *y*-axis is normalized to the total number of analyses (*n*). Core Phe(a), core Phe(b), mantle M1, mantle M2 and rim indicate the Si contents of phengite developed during the different growth stages identified by Ferraris *et al.* (2005).

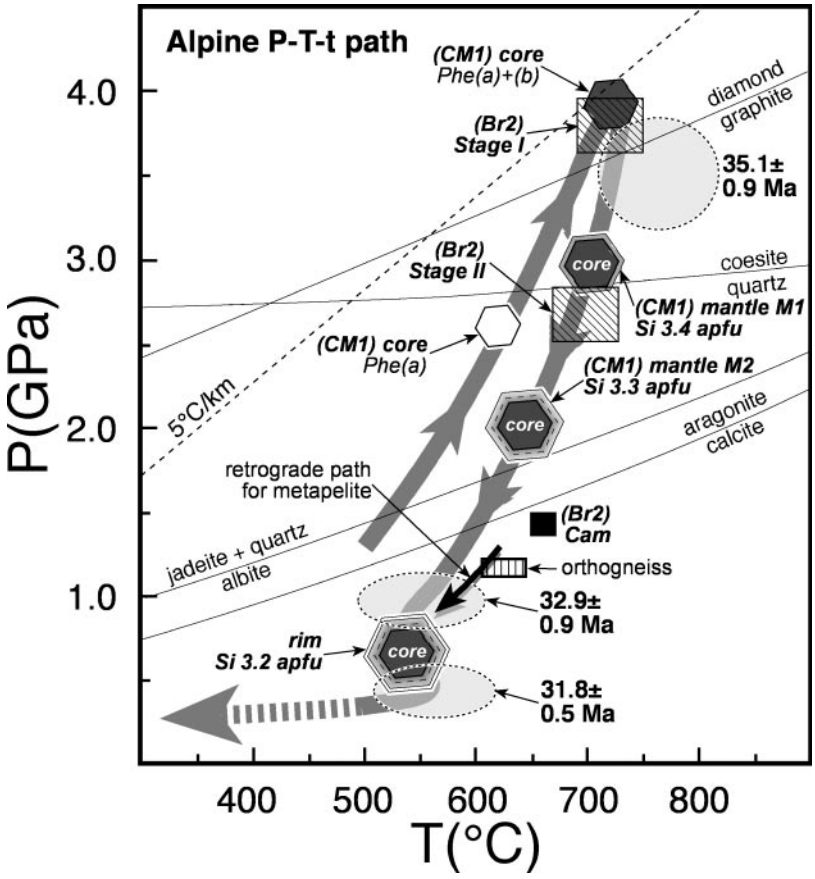

Fig. 5. Alpine metamorphic evolution in *P–T* space recorded in impure marble CM1 and phengite eclogite Br2. Prograde, peak and decompressional growth stages of phengite crystals from the marble are from Ferraris *et al.* (2005) and are shown schematically (see text for further details). Boxes are the equilibration conditions estimated from the garnet–clinopyroxene–phengite geothermobarometer of Ravna & Terry (2004) for peak (Br2 Stage I) and decompressional (Br2 Stage II) stages in eclogite Br2. *P–T* conditions estimated for the growth of later amphibole in the phengite eclogite (Br2 Cam) are indicated with a black square. The grey path is the Alpine *P–T* path of the BIU estimated by Compagnoni *et al.* (1995), modified on the basis of peak *P–T* estimates (Castelli *et al.*, 2004) in a garnet–clinopyroxene–phengite–rutile marble from Costa Monforte. The black arrow shows a portion of the retrograde path reported by Groppo *et al.* (2006) for a metapelite of the BIU, and the box with vertical lines the *P–T* conditions estimated by Groppo *et al.* (2005) for an orthogneiss compositionally comparable with samples D1 and D2. The grey dashed circles are the Alpine *P–T* estimates with 2σ errors of the UHP and of the two retrograde stages dated by Rubatto & Hermann (2001). The diamond ⇔ graphite, coesite ⇔ quartz, jadeite + quartz ⇔ albite, and aragonite ⇔ calcite reactions have been calculated using the thermodynamic database of Holland & Powell (1998, upgrade 2002).

increases [e.g. from 0·7 to ∼7 ppm along the profile rim(a)–core], with a progressive increase in the mantle and core domains (Si >3·3 a.p.f.u.) and an abrupt increase at the outer rim, corresponding to the last few tens of micrometres of the grain (Fig. 6). Such a variation is in agreement, in terms of both major element and Sr contents, with that detected in profile rim(b)–core (Fig. 6), where the lowest Si content in the rim region closely corresponds to that of mantle M2 phengite, and the Sr content reaches ∼2 ppm. From the core to the border of the grain, Rb contents [analyses 1a to 5a (Table 2 and Fig. 6)] first increase slightly (from 347 to 381 ppm) and then decrease (to 295 ppm). As for the other elements, although with different depletion–enrichment factors, Li, Zr and Ba increase from the core to the rim, B, F, Cr and Cs decrease, whereas K, Ti and V remain nearly constant (Fig. 6 and Table 2). Analysis by secondary ion mass spectrometry (SIMS) therefore shows that besides major element zoning, the investigated phengite from marble CM1 preserves a pronounced zoning in trace elements. The antipathetic behaviour of Rb and Sr produces a dramatic variation in the Rb/Sr ratio, which decreases by more than a factor of 10 moving from the core to the rim (from ∼525 to ∼42, Table 2).

Sample Br2—eclogite

Sample Br2 is a phengite eclogite collected from a mafic body, a few metres in length and less than 1 m thick, enclosed in paraschists of the polymetamorphic complex

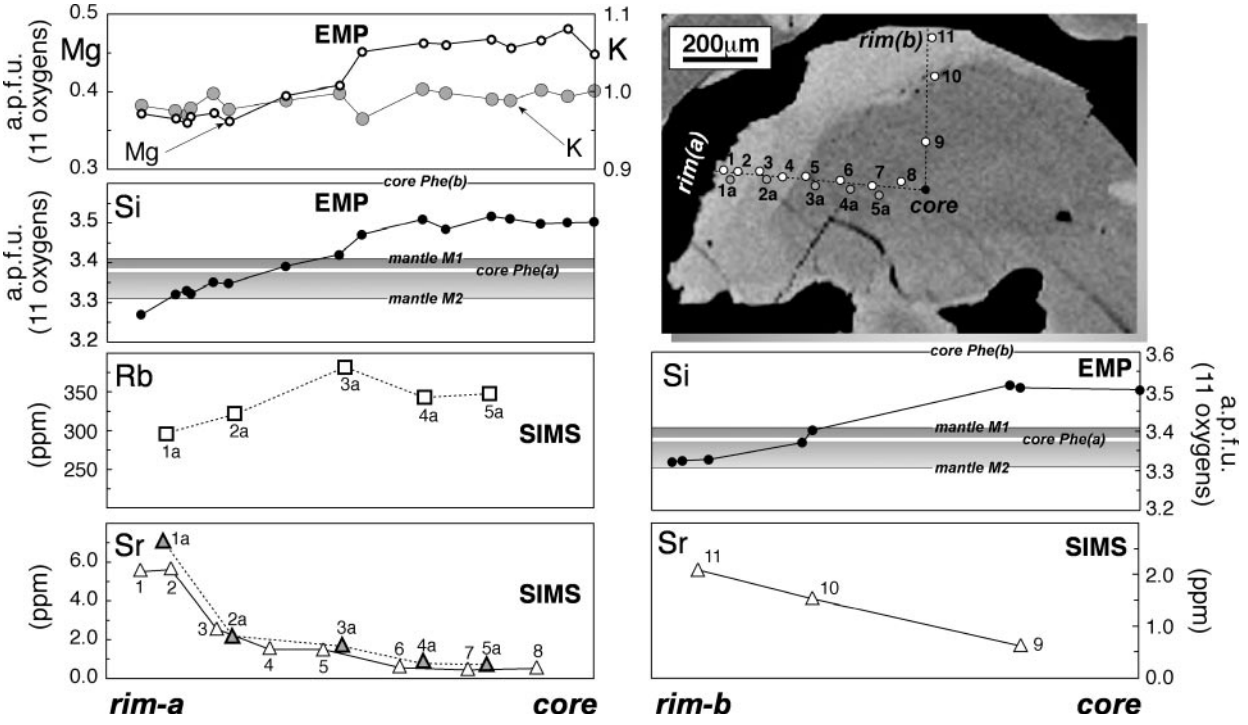

Fig. 6. Core to rim trace and major element variations in phengite grain (3) shown in Fig. 4.

(Fig. 1). Petrological data on this body have already been reported by Kienast *et al.* (1991), and comparable lithologies have been studied by Nowlan *et al.* (2000). Eclogite Br2 is fine to medium grained and consists of omphacite, garnet, phengite, amphibole, quartz and rutile. A very fine-grained symplectite consisting of clinopyroxene and plagioclase, locally and partially replaces omphacite. Phengite is very rarely replaced along the outermost rim (corresponding to the last few tens of micrometres of the flake) by a very fine-grained symplectite consisting of plagioclase and biotite. The alignment of omphacite and phengite flakes defines a foliation that most probably formed at or close to the UHP peak stage (e.g. see Michard *et al.*, 1995). Amphibole mainly occurs as porphyroblasts a few millimetres in size, locally enclosing garnet and, more rarely, omphacite relics. Phengite ranges in length from a few hundred micrometres to a few millimetres, and exhibits a highly variable Si content of ~3·6 to ~3·3 a.p.f.u. (locally to ~3·2 a.p.f.u; Table 1), in fairly good agreement with Si contents in phengites of marble CM1 (Fig. 3). Larger flakes are nearly homogeneous (Si ≥3·5 a.p.f.u.) and show a general decrease in celadonite content along grain boundaries (Fig. 7a). Smaller grains commonly exhibit lower Si contents, which are comparable with, or are lower than, those detected in the rim regions of the larger flakes. Grains of the 0·16–0·25 mm fraction exhibit Si contents predominantly higher than 3·35 a.p.f.u. As for *P–T* conditions, using garnet ($Alm_{45}Pyp_{26}Grs_{27}Sps_2$) and omphacite ($Jd_{53}Di_{41}Hd_5Ae_1$) core compositions and the phengite with the highest celadonite content [Si 3·61 a.p.f.u. and Mg/(Mg + Fe) 0·86], the geothermobarometer of Ravna & Terry (2004) yielded a temperature of ~720°C and a pressure of ~3·7 GPa (Stage I in Fig. 5). These values are comparable with peak stage II documented by Nowlan *et al.* (2000). Garnet ($Alm_{49}Pyp_{28}Grs_{22}Sps_1$) and omphacite ($Jd_{47}Di_{43}Hd_{10}Ae_0$) inner rim compositions and lower celadonitic phengites [Si 3·32 a.p.f.u. and Mg/(Mg + Fe) 0·74] gave a temperature of ~700°C and a pressure of ~2·7 GPa (Stage II in Fig. 5), comparable with the retrograde stage III documented by Nowlan *et al.* (2000). Late amphibole porphyroblasts are mainly magnesiokatophorites and locally, along the rim, edenite–pargasites (nomenclature after Leake *et al.*, 1997; Table 1). They are compositionally comparable with amphiboles experimentally obtained by Schmidt (1993) in the tonalitic system at ~1·4 GPa and 650°C [stage Br2(Cam) in Fig. 5], in agreement with the physical conditions suggested by Michard *et al.* (1995).

Samples D1 and D2—orthogneiss

Samples D1 and D2 are medium- to fine-grained granitic gneisses with augen structure (Fig. 1). They consist of quartz, albite, K-feldspar, white mica, biotite and epidote (locally overgrown on allanite), and accessory garnet,

Table 2: SIMS data (concentrations in ppm) on a selected phengite grain [grain(3)–Fig. 6] from marble CM1

	Analytical session 1										
	rim-a							core			rim-b
	1	2	3	4	5	6	7	8	9	10	11
Sr	5·6	5·7	2·6	1·6	1·5	0·6	0·5	0·6	0·6	1·5	2·1

	Analytical session 2				
	rim-a				core
	1a	2a	3a	4a	5a
Li	150	134	97	96	79
Be	4·8	3·8	4·4	4·0	4·1
B	30	34	40	45	56
F	772	724	896	924	978
Sc	5	5	6	4	5
Ti	1751	1808	1736	1778	1747
V	111	111	110	105	108
Cr	2	4	3	8	8
Rb	295	321	381	342	347
Sr	7·1	2·1	1·7	0·8	0·7
Zr	1·1	0·4	0·5	0·7	0·3
Nb	10·5	7·4	11	9·4	8·1
Cs	8	8	19	17	17
Ba	1547	1077	992	999	861
Rb/Sr	42	150	228	444	526

titanite, apatite and zircon. White mica consists of millimetric fish or reoriented grains enveloped by a new foliation defined by smaller white mica and biotite flakes. Biotite is locally chloritized or exhibits pronounced parting along the basal cleavage. Compared with those of the marble and eclogite (Fig. 3), white micas from the orthogneisses show a narrower range in celadonite content (Si content of 3·5–3·24 a.p.f.u.; Table 1), a lower maximum Si content, and lower Mg and higher Fe contents (0·29–0·18 and 0·39–0·24 vs 0·55–0·24 and 0·07–0·16 a.p.f.u., respectively). Larger grains are zoned and cover the whole compositional range, with a general decrease in celadonite from the core to the rim (Fig. 7). Smaller grains show lower celadonite contents and narrower compositional variations (Si $\leq$3·35 a.p.f.u.). The occurrence of albite and the low Si content in phengite for the limiting assemblage phengite + K-feldspar + biotite + quartz (Massonne & Schreyer, 1987) suggest that these rocks totally re-equilibrated under lower *P–T* conditions during exhumation (starting from ~1·2 GPa at ~600°C). These physical conditions agree with the temperature of ~600°C and pressure of ~1·2 GPa indicated in a *P–T* pseudosection recently reported by Groppo *et al.* (2005) for the assemblage quartz + albite + microcline + phengite (Si 3·45 a.p.f.u.) + garnet + biotite + epidote ($a_{H_2O} = 0·75$) in a granitic orthogneiss from the BIU.

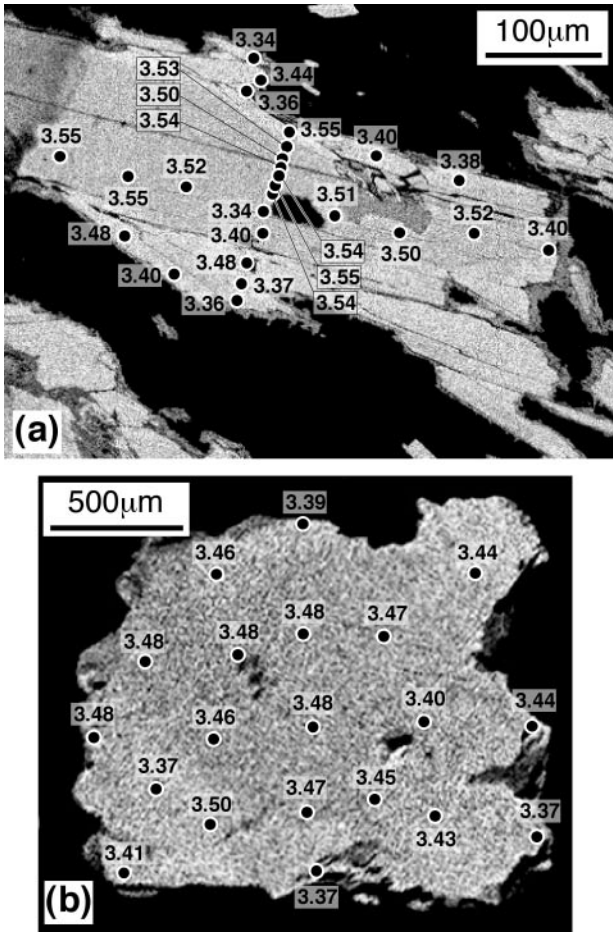

Fig. 7. Compositional variations (expressed as Si content a.p.f.u.) reported on X-ray maps of Al in phengite from eclogite Br2 (a) and orthogneiss D1 (b).

ISOTOPIC DATA

Rb–Sr dating

Sample CM1—phengite marble

Rb–Sr data points (whole-rock, calcite and five phengite fractions) do not define a single linear array in an isochron diagram (Fig. 8a), thus documenting strong within-sample isotopic disequilibrium. Data from the various phengite fractions regressed with those for calcite

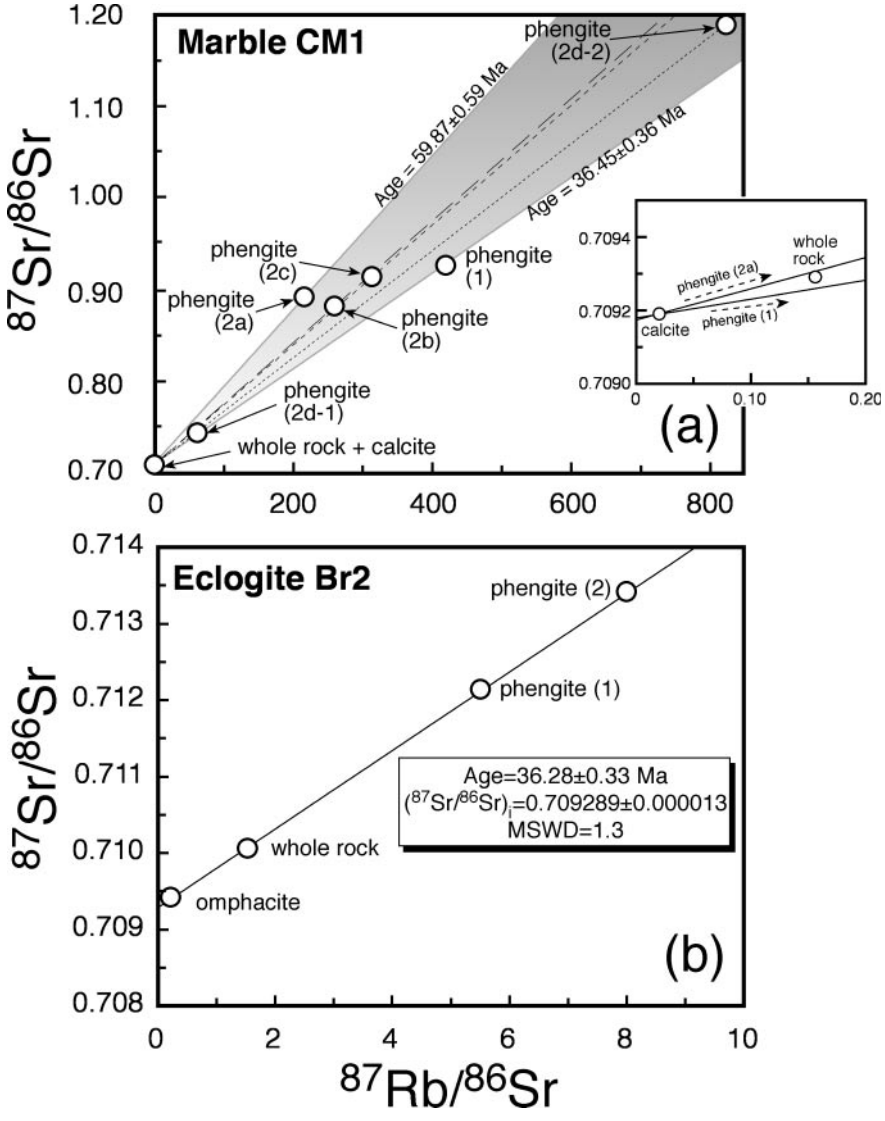

Fig. 8. Rb–Sr isochron diagrams for marble CM1 (a) and eclogite Br2 (b). Error bars are within the size of the plot symbols.

(Fig. 8a and Table 3) yield apparent ages ranging from 36·45 ± 0·36 Ma [wet-ground 0·16–0·25-mm grain fraction (1)] to 59·87 ± 0·59 Ma [unground >0·50 mm grain fraction (2a)]. Phengite fractions (2b) and (2c) gave comparable two-point (phengite–calcite) apparent ages of 46·80 ± 0·46 and 46·05 ± 0·45 Ma, respectively. However, they fail to produce a statistically acceptable three-point isochron when regressed with calcite (MSWD = 5·2). In Fig. 8a phengite fractions (1), (2a), (2b) and (2c) define a trend with a gentle positive slope, apparently documenting a negative correlation between the Rb–Sr apparent age and Rb/Sr elemental ratio. The two splits [the <0·10 mm (2d-1) and >0·25 mm (2d-2) grain size] recovered after wet grinding of a fourth >0·50 mm fraction, despite the only marginally different apparent ages calculated with respect to calcite data [39·39 ± 0·40 and 41·10 ± 0·40 Ma for split (2d-1) and (2d-2), respectively], yielded contrasting results. They have markedly different Rb/Sr and $^{87}Sr/^{86}Sr$ ratios (Table 3 and Fig. 8a), with the coarser fraction (2d-2) yielding the highest Rb/Sr and $^{87}Sr/^{86}Sr$ ratios, even with respect to the other analysed phengite fractions. It is also characterized by a very low Sr content (~1 ppm), comparable with that detected in the core region of phengite grain (3) (Table 2 and Fig. 6). In contrast, the smallest fraction (2d-1) has much lower Rb/Sr and $^{87}Sr/^{86}Sr$ ratios, suggesting contamination by calcite. Rb and Sr contents in the analysed phengites, except for Sr in fraction (2d-1), are comparable with those determined by SIMS analysis (Table 2).

Table 3: Rb-Sr analytical results

Sample	Rb (ppm)	Sr (ppm)	$^{87}Rb/^{86}Sr$	$^{87}Sr/^{86}Sr$	$\pm 2\sigma_m$
Marble CM1					
whole rock	7·77	144	0·156	0·709292	0·000013
calcite	0·93	133	0·0203	0·709190	0·000012
phengite* 0·16–0·25 mm (1)	453	3·19	420·2	0·926730	0·000020
phengite >0·50 mm (2a)	408	5·59	215·4	0·892380	0·000013
phengite >0·50 mm (2b)	363	4·10	260·5	0·882340	0·000080
phengite >0·50 mm (2c)	405	3·81	313·8	0·914433	0·000027
phengite* >0·50 mm (2d-1)	382	18·0	61·68	0·743692	0·000081
phengite* >0·50 mm (2d-2)	311	1·15	822·2	1·18915	0·00049
Eclogite BR2					
whole rock	67·5	128	1·528	0·710065	0·000010
omphacite	8·84	116	0·221	0·709410	0·000010
phengite* 0·16–0·25 mm (1)	409	215	5·506	0·712131	0·000009
phengite >0·5 mm (2)	414	150	7·998	0·713416	0·000010

*Wet ground for few minutes using an agate mortar and pestle grinder. After grinding, fraction (2d) was further sieved; (2d-1) represents the grain size <0·10 mm and (2d-2) that >0·25 mm.

Sample Br2—eclogite

Data from the whole-rock, omphacite and the two phengite fractions [the wet-ground 0·16–0·25 mm grain fraction (1) and the unground >0·50 mm fraction (2)] give a well-defined least-squares fit (MSWD = 1·3) with an age of 36·28 ± 0·33 Ma (Fig. 8b), thus attesting to within-sample isotopic equilibrium. This age agrees strikingly with the two-point calcite–phengite (1) age obtained from sample CM1.

^{40}Ar–^{39}Ar dating

Sample CM1—phengite marble

Laser step-heating experiments on bulk phengite (0·16–0·25 mm grain fraction) and on a single millimetre-sized phengite grain yield reproducible, internally discordant age patterns (Fig. 9a) with an overall hump shape and increasing apparent ages in the final steps. Data from the bulk sample, however, yield younger apparent step ages than those from the single grain (~40–45 Ma vs ~49–55 Ma; Fig. 9a and Appendix Table A, available as Supplementary Data on the *Journal of Petrology* web site at http://www.petrology.oxfordjournals.org), which are reflected in the total gas ages of 42·65 ± 0·24 and 52·90 ± 0·27 Ma (Fig. 9a). The apparent ages from *in situ* data on larger flakes range from ~35 to ~62 Ma, with a general decrease in age from the core to the rim, and are comparable for both crystal orientations (Fig. 10a). Apparent ages from *in situ* data encompass the time interval defined by step-heating analysis, and the whole dataset derived from the two different extraction techniques, when taken at face value, is in apparent agreement with the age interval defined by Rb–Sr data (~36–60 Ma). Fifteen analyses on grain a-1 (Fig. 10a) give a total gas age of 50·9 ± 0·4 Ma, in striking agreement with the total gas ages of the single grain analysed through the incremental heating technique. Sub-millimetric grains in the rock chip give apparent ages younger than ~50 Ma (Appendix Table B, available as Supplementary Data on the *Journal of Petrology* web site). Ar data from both laser step-heating and *in situ* experiments have low to very low $^{37}Ar_{Ca}$ and $^{38}Ar_{Cl}$ intensities (Appendix Tables A and B in the Supplementary Data), and consequently low Ca/K and Cl/K ratios, which agree with the mica chemistry and suggest negligible contamination by extraneous phases. Two areas ($100 \times 500\ \mu m^2$) sampled in calcite by the ultraviolet (UV) laser yielded unrealistically old apparent ages of 7·4 ± 5·5 and 4·6 ± 1·2 Ga (Appendix Table B in the Supplementary Data).

Sample Br2—eclogite

Laser step-heating analyses were carried out on a multigrain phengite fraction (0·16–0·25 mm fraction), a single millimetre-sized phengite grain, and on one amphibole separate (Appendix Tables A and B in the Supplementary Data). Data from both the bulk phengite and the single grain yielded discordant age profiles, with apparent step ages significantly older than the Ar ages from CM1 phengite. The bulk phengite sample yields a declining profile for the first ~70% of the total $^{39}Ar_K$ released, with apparent step ages varying from ~133 to ~118 Ma, followed by a hump with apparent ages of up to ~139 Ma (Fig. 9b). The single grain has a much less disturbed spectrum, with an overall declining shape with increasing temperature, and apparent ages of 198 ± 24 Ma (first step) to 137·9 ± 1·4 Ma. Steps 4–8 are concordant at 2σ analytical uncertainty, represent ~69% of the total $^{39}Ar_K$ released, and yield a weighted-mean apparent age of 139·0 ± 1·0 Ma. However, the resolution of the step-heating experiment on the single phengite grain is limited by step 4, which gave a large gas yield corresponding to ~63% of the total $^{39}Ar_K$ released. Total gas ages are 122·0 ± 0·6 and 139·9 ± 0·9 Ma for the bulk sample and the single grain, respectively (Fig. 9b). As in the case of step-heating runs on CM1 phengite, significantly older apparent ages were obtained for the millimetre-sized single grain than for the smaller-sized bulk sample. ^{40}Ar–^{39}Ar *in situ* laser ages on phengite extend the time interval defined by step-heating experiments to both younger and older apparent ages (~89–170 Ma; Fig. 10b). Age mapping shows that the youngest apparent

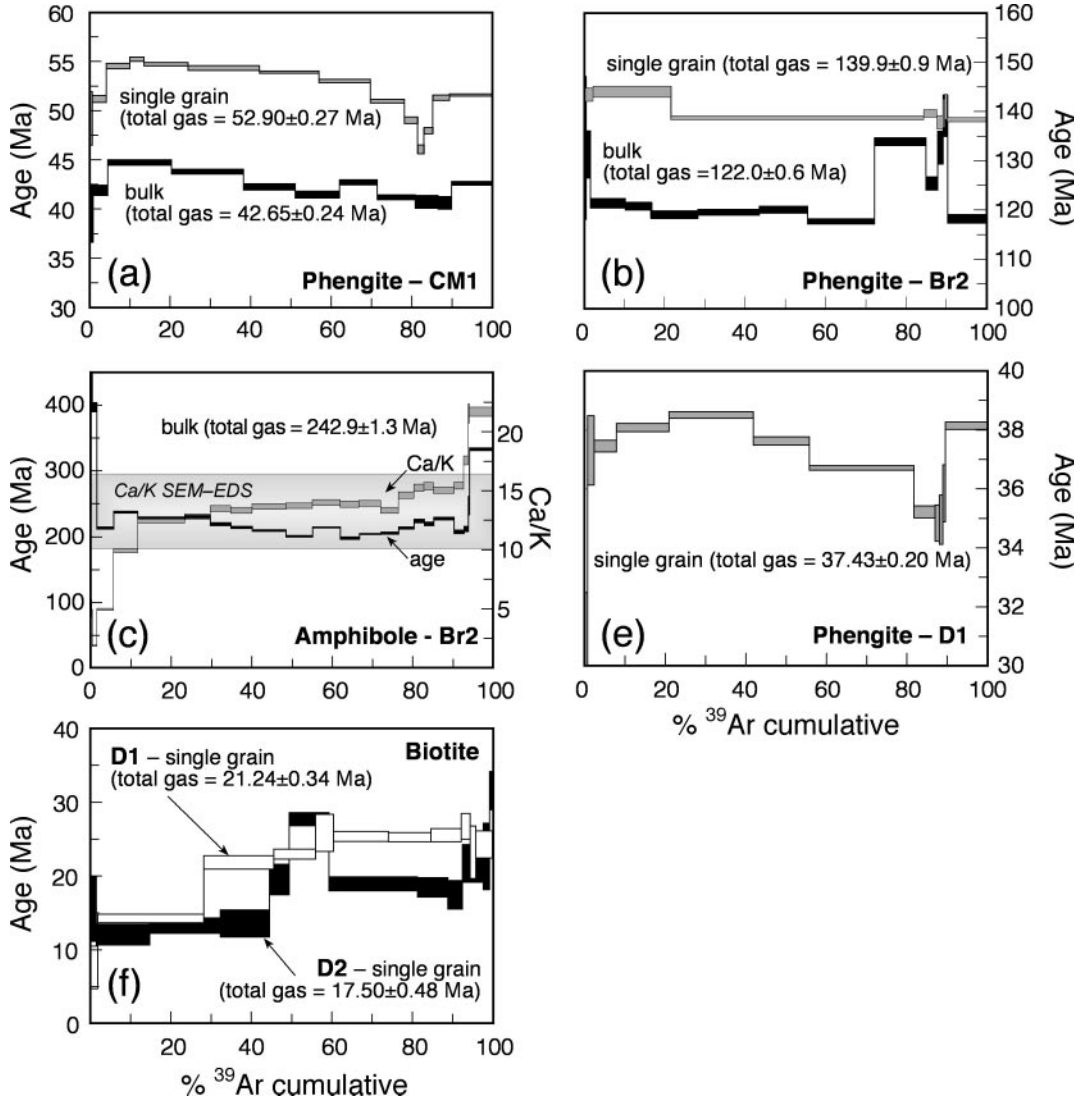

Fig. 9. Age release spectra of phengites (samples CM1, Br2, D1), amphibole (sample Br2) and biotites (samples D1, D2). (c) also shows the Ca/K release spectrum (derived from neutron-produced $^{37}Ar_{Ca}$ and $^{39}Ar_K$). The grey field in (c) shows the variation of Ca/K ratios determined by SEM–EDS analysis on amphibole in polished thin sections.

ages correspond to the rims of millimetric flakes or to smaller (sub-millimetric) grains (Fig. 10b and Appendix Table B in the Supplementary Data). *In situ* analyses carried out along the length of the phengite grains in the rock chip yield the widest interval of apparent ages (Fig. 10b). Total gas ages derived from the three grains shown in Fig. 10b range from 130·8 ± 0·9 to 142·6 ± 0·9 Ma. Although these apparent ages are comparable with the total gas age from incremental heating analysis of the single grain, they are slightly older than the total gas age from incremental heating analysis of the bulk sample. Ca/K and Cl/K ratios are very low in the whole dataset (Appendix Tables A and B in the Supplementary Data), once again suggesting that pure phengite was analysed.

The amphibole separate was degassed over 25 steps to obtain the most detailed age profile possible. On the whole, the apparent age spectrum shows a saddle shape (Fig. 9c) characterized by unrealistically old ages in the low-temperature steps (3·7–2·1 Ga; Appendix Table A in the Supplementary Data), ages scattered within the ~237–198 Ma interval from step 6 to step 23, and increasing ages in the final steps (to ~333 Ma). All apparent step ages are significantly older than the apparent ages obtained for phengite. The Ca/K ratio derived from Ar isotopes (Fig. 9c) initially increases, then almost stabilizes at values (~13–15) typical of amphibole according to SEM–EDS analysis (Fig. 9c), before increasing again (to ~22) in the remaining ~20% of the released $^{39}Ar_K$. The low Ca/K ratios in the low-temperature

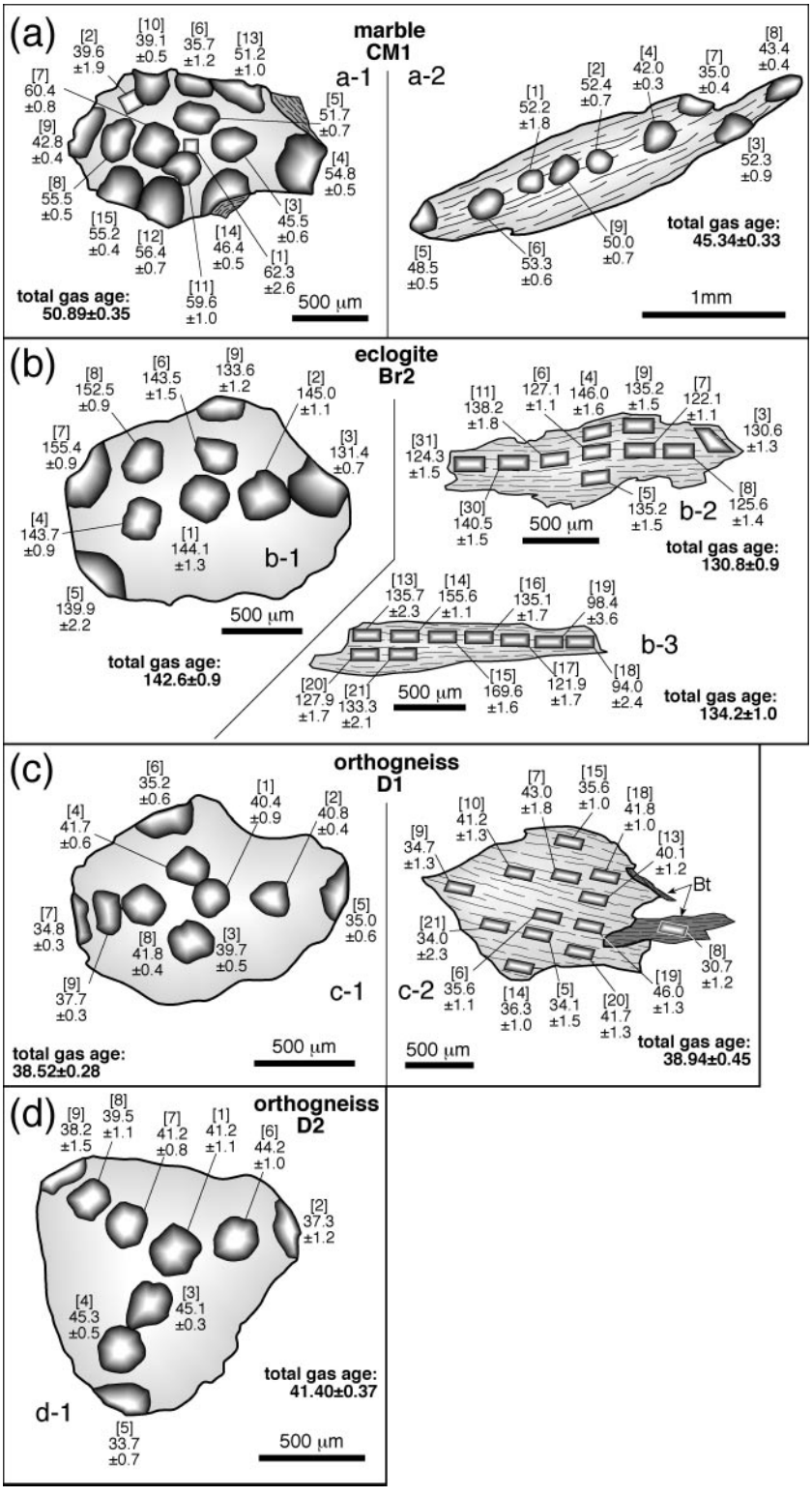

Fig. 10. Line drawings showing the distribution of ^{40}Ar–^{39}Ar apparent ages (Ma) from *in situ* analyses in phengite within marble CM1 (a), eclogite Br2 (b), and orthogneisses D1 (c) and D2 (d). Grains a-1, b-1, c-1 and d-1 were recovered from the >0·50 mm grain fraction and analysed on the cleavage plane. Grains a-2, b-2, b-3 and c-2 were analysed instead along the length of mica grains (i.e. parallel to the basal cleavage) in rock chips. Circular melt pits were obtained using the IR laser, and rectangular pits by rastering the UV laser. Numbers in brackets correspond to the analysis number of Appendix Table B in the Supplementary Data. Analysis numbering reflects the data sampling sequence in time. Errors are 2σ.

steps suggest the presence of minor K-rich impurities (phyllosilicates), whereas the slight increase at high temperature may indicate minor contamination by a high-Ca mineral phase, probably omphacite. Three infrared (IR) multi-spot measurements on amphibole in the rock chip yielded apparent ages of ~117 to 162 Ma (Appendix Table B in the Supplementary Data), younger than those from step-heating analysis. The low Ca/K ratios (3·1–9·4), however, suggest that these data are unreliable because of contamination by phengite.

Samples D1 and D2—orthogneiss

Laser step-heating analysis of a single millimetre-sized phengite grain from sample D1 (Fig. 9e) yields an age spectrum remarkably similar in shape to that of phengites from marble CM1. Apparent step ages, however, are significantly younger and range from ~38·5 to ~35 Ma (Fig. 9e). *In situ* analyses from samples D1 and D2, when compared with the incremental heating experiment on the single grain, span a larger interval characterized by comparable minimum apparent ages but older maximum apparent ages (up to 46·0 ± 1·6 and 53·0 ± 1·3 Ma for samples D1 and D2, respectively; Appendix Table B in the Supplementary Data). Figures 10c and 10d show that millimetre-sized grains analysed on the cleavage plane (grains c-1 and d-1), and one mica fish (grain c-2) within the rock chip, analysed parallel to the basal cleavage, display similar age variations and comparable intra-grain Ar age distributions with a well-defined core–rim relationship.

Two step-heating experiments on single biotite grains from both samples yielded discordant internal age spectra with an overall rising trend (Fig. 9f). Maximum apparent ages for biotite in D1 and D2 are 25·5 ± 0·9 and 31·6 ± 2·6, respectively. However, the high atmospheric Ar content (in most steps ≥50 %) and the high Ca/K ratios (Appendix Table A in the Supplementary Data) suggest that the results are unreliable, probably as a result of chloritization. ^{40}Ar–^{39}Ar apparent ages for biotite determined by *in situ* analysis within the rock chips range widely, are positively correlated with atmospheric Ar contents (Appendix Table B in the Supplementary Data) and agree reasonably well with the apparent ages from step-heating analysis. Following the results of other studies on chloritized biotites (Di Vincenzo *et al.*, 2003, and references therein), the oldest *in situ* ages of 30·7 ± 1·2 and 29·8 ± 1·2 Ma (for samples D1 and D2, respectively), characterized by the highest radiogenic Ar contents, are taken as the best minimum estimate for the true biotite age in the studied orthogneisses. These ages agree with those (28–34 Ma) reported for biotites in comparable lithologies (Monié & Chopin, 1991) and zircon ages from fission-track data from the pyrope whiteschists (Gebauer *et al.*, 1997).

DISCUSSION

Limited fluid mobility and consequences for isotope transport in UHP rocks

Studies on stable isotopes and fluid inclusions have shown that most UHP and HP rocks evolved as a closed system, in which limited aqueous fluids with restricted mobility were available only transiently and episodically when released by dehydration reactions (see, e.g. Philippot & Rumble, 2000, and references therein). The limited and episodic availability of fluids clearly has a profound impact on the kinetics of both metamorphic reactions and isotopic transport. In the absence of free aqueous fluids, even minerals such as trioctrahedral micas, which are prone to resetting irrespective of the effective isotope loss mechanism (including volume diffusion, recrystallization, alteration etc.; Dahl, 1996), may preserve isotope records through temperatures exceeding the commonly assumed T_c by hundreds of degrees (Verschure *et al.*, 1980; Kelley & Wartho, 2000; Kühn *et al.*, 2000; Maurel *et al.*, 2003).

As for white mica developed in mafic rocks under HP conditions, Glodny *et al.* (2003) proposed a close analogy between the kinetic role of fluids in metamorphic reactions and in isotope redistribution, with the implication that preservation of petrographic relics ensures isotope inheritance. They suggested that certain assemblages (e.g. omphacite–garnet-dominated eclogites) preserve their Rb–Sr isotopic signature as long as they remain isolated from free fluids, and that only fluid–rock interaction may cause isotope re-equilibration. Additionally, their statistically well-defined least-squares fits in isochron diagrams for samples with eclogite-facies assemblages imply local Sr isotope equilibrium at least on the length scale of the specimen used for mineral separation (<100 g).

As for K–Ar systematics, the possibility that the mobility of radiogenic Ar is strictly linked to that of structure-forming major elements was discussed by Villa (1998) and demonstrated in several studies on natural examples that had experienced not only extreme physical conditions (e.g. UHP–HP conditions; Giorgis *et al.*, 2000; Di Vincenzo & Palmeri, 2001; Di Vincenzo *et al.*, 2001; Agard *et al.*, 2002) but also more ordinary *P*–*T* regimes (Hammerschmidt & Frank, 1991; Hames & Cheney, 1997; Villa *et al.*, 2000; Di Vincenzo *et al.*, 2004). From a general standpoint, because of their large diameter and inertness, Ar atoms tend to preferentially partition into fluid phases, with the implication that the fate of Ar is strictly linked to the evolution of fluids. In a closed system characterized by the reduced mobility of internally derived fluids, the Ar isotope composition of grain

boundary fluids will, therefore, reflect the integrated age and potassium content of the protolith (Foland, 1979; Scaillet, 1998; Kelley, 2002; Sherlock & Kelley, 2002). Under UHP conditions, however, the presence of highly saline fluids [e.g. as documented for pyrope whiteschists and the host orthogneiss of the BIU by Philippot *et al.* (1995)] may further hinder Ar mobility, given the well-known decrease in Ar solubility with increasing salinity of aqueous fluids [see, e.g. Scaillet (1998) and Kelley (2002) and references therein]. This means that under high Ar concentrations, grain boundary fluids consisting of highly saline brines are inefficient carriers of Ar in UHP–HP terrains, even on a local scale (Scaillet, 1998).

It should be noted that under closed-system conditions, with isotope exchange limited to a small scale, there exists an intrinsic difference between the K–Ar dating technique and techniques based on the internal mineral isochron approach (Rb–Sr in the present study). In the case of Rb–Sr, the effect of excess radiogenic Sr is potentially annulled by the attainment of local isotope equilibrium: partitioning excess Sr among minerals of a particular equilibrium assemblage gives rise to a common initial isotopic composition. In contrast, a potassic mineral phase nucleating in local equilibrium with a fluid phase containing excess Ar will incorporate variable amounts of parentless Ar according to the partition coefficient between the mineral and the grain boundary fluid and to the concentration of parentless ^{40}Ar in the whole-rock system. The partition coefficient is, in turn, controlled by Ar solubility in that mineral [a function of its crystal–chemical features; e.g. for micas see Dahl (1996)] and in the fluid phase. In the present case, following the definition of Lanphere & Dalrymple (1976), although parentless ^{40}Ar is internally derived, it does not represent genuine inherited Ar because it is not strictly related to the physical presence of an older mineral phase.

Dehydration vs hydration behaviour of different lithologies

Proyer (2003) outlined the importance of linking the dehydration behaviour of a particular lithology, when subjected to UHP–HP regimes, to the P–T conditions they are able to preserve. He showed that metagranites do not easily record or preserve high-pressure conditions, because they need infiltration of external fluids to re-equilibrate under eclogite-facies conditions. During exhumation, the same reactions cause internal dehydration and, as a consequence, the pervasive re-equilibration of the rock at upper crustal levels. In contrast, eclogites, ultramafites and marbles undergo continuous dehydration reactions along the prograde path, but most decompressional paths crosscut hydration reactions, which require infiltration of external fluids for re-equilibration to occur (Proyer, 2003, and references therein).

This situation is paralleled by the studied samples from the BIU. Although orthogneisses D1 and D2 spent a significant portion of their prograde and retrograde path in the jadeite + quartz stability field, they totally re-equilibrated in the albite stability field and now lack any evidence of the UHP stage. The Fe-rich and relatively celadonite-poor phengites re-equilibrated at upper crustal levels, and cannot be directly compared from a chronological viewpoint with the Mg-rich phengites of the eclogite and marble. Indeed, both eclogite Br2 and marble CM1 record different portions of the P–T path of the BIU, including a segment of the prograde path, as revealed by the TEM investigation of phengites in the marble (Ferraris *et al.*, 2005). Given the lack of an *ad hoc* study at the sub-micrometre scale, available data cannot be used to determine whether the cores of matrix phengites in the eclogite also retain a record of the prograde path; consequently, it is impossible to establish whether phengites with the highest celadonite contents represent the average of prograde and peak phengites, as observed in the marble, or whether they correspond to a pure UHP end-member. Nowlan *et al.* (2000) reported prograde low-Si phengites preserved as armoured relics only in the core region of garnets characterized by low Mg contents. It should be noted, however, that high-Si phengite cores from large crystals in the matrix, along with coexisting omphacite and garnet compositions, yield physical conditions [Nowlan *et al.* (2000) and data from the present work] in agreement with those determined for the UHP stage in other lithologies on the basis of different geothermobarometers. It is thus more likely that analyses with the highest celadonite contents correspond to a UHP end-member phengite rather than to a mixture of prograde and peak phengite as observed in the marble.

The above arguments suggest that the studied orthogneisses were most probably infiltrated by externally derived fluids (i.e. during burial to UHP conditions), whereas both the eclogite and marble generally were not, except for limited late hydration in the eclogite evidenced by the growth of late amphibole. As for the marble, Ferraris *et al.* (2005) pointed out the difficulty in obtaining reliable pressure estimates using the Si content in phengite, given the lack of evidence in the studied marble for buffering of the celadonite substitution. They proposed a crystallization pressure of ~2·6 GPa for the prograde phengite [Phe(a)] and a pressure of ~3·9 GPa for the peak phengite [Phe(b)] on the basis of the thermobarometric estimates reported by Castelli *et al.* (2004). Ferraris *et al.* (2005) reported qualitative crystallization pressures of ~3·0 to ~2·0 GPa for the mantle phengites, and of ~0·4 GPa for the rare and discontinuous low-celadonite rims. Crystallization pressures for phengites in eclogite Br2 are better constrained using conventional geothermobarometry, indicating that phengite mostly nucleated

and/or re-equilibrated from the UHP peak down to ~2·7 GPa. In contrast, as stated earlier, orthogneisses totally re-equilibrated at upper crustal levels, and Si contents in phengite (3·50–3·25 a.p.f.u.) for the limiting assemblage phengite + K-feldspar + biotite + quartz (Massonne & Schreyer, 1987) suggest pressures of approximately 1·2 to 0·7 GPa.

Excess or inherited isotopic components and meaning of isotopic ages

Even ignoring temporal constraints for BIU derived from U–Pb SHRIMP data, some of the apparent Ar ages from the studied samples are no doubt clearly plagued by excess Ar and are geologically meaningless. For instance, the ^{40}Ar–^{39}Ar ages from phengites of the eclogite (up to ~170 Ma) vastly exceed the Rb–Sr phengite age from the same sample or the sequence of ages in eclogite Br2, with phengite yielding ages significantly younger than those from amphibole, even though amphibole is a texturally late phase, strongly suggest contamination by parentless ^{40}Ar. Conversely, Rb–Sr data from eclogite Br2 yielded an isochron age of 36·28 ± 0·33 Ma, which overlaps within error limits with the 35·4 ± 1·0 Ma age reported by Gebauer *et al.* (1997) for zircons extracted from pyrope megablasts of the whiteschists, and with the 35·1 ± 0·9 Ma age reported by Rubatto & Hermann (2001) for titanite formed under UHP conditions. A rigorous comparison with the U–Pb data, however, should take into account that, first, phengite from the eclogite is compositionally heterogeneous and records the portion of the *P–T* path experienced by the BIU from metamorphic peak to ~2·7 GPa (i.e. corresponding to the first 20–30 km of exhumation) and, second, that the decay constants involved in the U–Pb dating method are known with much better accuracy than that of ^{87}Rb (Begemann *et al.*, 2001). ^{40}Ar–^{39}Ar data from both the eclogite and marble show a general decrease in age from the core to the rim of millimetric grains. They also show older total gas ages from both step-heating and *in situ* analysis of millimetric grains than from step-heating analysis of the smaller-sized grain fractions (0·16–0·25 mm). This evidence indirectly suggests that the mineral separation procedure effectively concentrated phengites with lower Si contents in the smaller grain fractions. Rubatto & Hermann (2001) derived a mean exhumation rate as high as 34 km/Ma from peak conditions to ~1 GPa. Given that exhumation of UHP rocks is essentially driven by buoyancy up to the middle crust (Chopin, 2003, and references therein), the exhumation rate may have been even faster in the first tens of kilometres from mantle depths. Therefore, possible Sr-isotopic disequilibria between the compositionally different phengite fractions may have been lost within analytical uncertainties, as supported by the well-defined fit for Rb–Sr data.

As far as the orthogneisses are concerned, taking into account petrological and Rb–Sr data from the eclogite and the *P–T–t* path reported by Rubatto & Hermann (2001), which suggest that the BIU reached the highest pressure conditions recorded by samples D1 and D2 (~1·2 GPa) at close to ~33 Ma, even phengites from the orthogneisses yielding ^{40}Ar–^{39}Ar *in situ* ages of ~50 to 35 Ma are variably contaminated by excess Ar. The only exception is the texturally late biotite, whose *in situ* minimum age of ~30 Ma is instead consistent with the final portion (from 0·5–0·4 to ~0·2 GPa, within ~32–30 Ma) of the decompressional *P–T–t* path reconstructed by Rubatto & Hermann (2001).

In contrast, the presence of prograde phengite relics in the marble requires that the first-order intra-sample concordance between Rb–Sr and ^{40}Ar–^{39}Ar ages of phengites be considered in light of all gathered data to assess whether it is internally consistent. As plate velocities most probably represent the limiting factor to burial rates during the prograde path of UHP rocks, it is implicit that the BIU may have required from a few million years to about 10 Ma to reach UHP peak conditions. For example, Lapen *et al.* (2003) recently hypothesized a minimum duration of 12 Ma for prograde garnet growth in the Zermatt–Saas meta-ophiolite (NW Alps), subducted to UHP conditions during Alpine convergence. Rb–Sr data from the marble CM1, yielding two-point (calcite–phengite) isochron ages of ~36 to 60 Ma (with two intermediate values of ~46–47 Ma), seem to be in too close agreement with the 35–60 Ma interval defined by ^{40}Ar–^{39}Ar data to be simply coincidental. However, it should be noted that Rb–Sr phengite ages are from bulk samples (several tens of grains for the >0·50 mm fractions), whereas the widest age interval of Ar data derives from spot analyses on single grains. Although total gas ^{40}Ar–^{39}Ar ages of around 50 Ma for the single millimetre-sized grains are comparable with the Rb–Sr ages of ~46–47 Ma from phengite fractions (2b) and (2c), they are much younger than the ~60 Ma Rb–Sr age from phengite fraction (2a). Given the very low Rb/Sr ratio of the marble system, even the pronounced intra-grain zoning of Sr contents, with a dramatic increase toward the rim (whose important implications will be discussed below), cannot explain the mismatch. On the other hand, the total gas age from step-heating analysis of the bulk phengite 0·16–0·25 mm fraction (~43 Ma) is significantly older than the Rb–Sr age (~36 Ma) from the same grain fraction; this leads us to conclude that ages from ^{40}Ar–^{39}Ar and Rb–Sr data do not entirely agree with each other. Furthermore, Rb–Sr data from phengite fractions (2b) and (2c), whose isochron ages fairly agree with ^{40}Ar–^{39}Ar total gas ages, are not consistent with other chemical data. Along with the finer-grained phengite (1), the three unground phengite fractions derived from the >0·50 mm grain size [i.e. (2a), (2b) and (2c)]

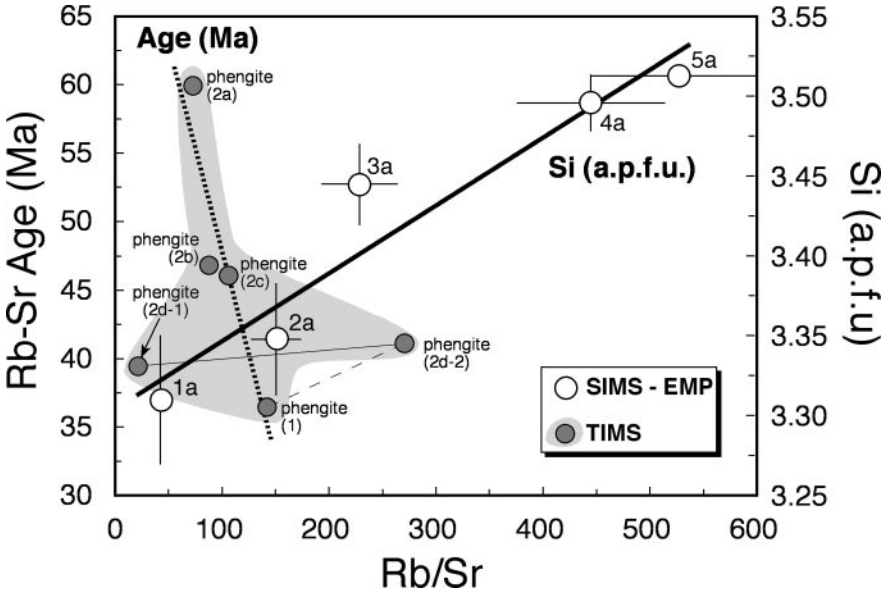

Fig. 11. Rb–Sr age and Si content (a.p.f.u.) vs Rb/Sr ratio for phengites of sample CM1. Numbers for SIMS–EMP data points refer to those reported for SIMS analysis in Fig. 6 and those for Rb–Sr data determined by TIMS (thermal ionization mass spectrometry) on the phengite fractions of Table 3. The bold dotted line shows the trend defined by the finer-grained phengite fraction [phengite (1)] and the three unground phengite fractions [(2a), (2b) and (2c)] derived from the >0·50 mm grain size. The bold continuous line shows the trend defined by SIMS and EMP data. The fine continuous line connects the <0·10 mm (2d-1) and >0·25 mm (2d-2) splits recovered after wet grinding of the fourth fraction handpicked from the >0·50 mm grain size. The fine dashed line connects the two fractions [phengite (1) and phengite (2d-2)] that were subjected to the wet-grinding and sieving procedure, and correspond to the purest fractions analysed.

define an apparent negative correlation between the Rb–Sr age and the Rb/Sr ratio (Fig. 11). This observation clearly contrasts with SIMS and EMP results, which instead support a concomitant decrease in celadonite content and Rb/Sr ratio from the core to the rim of the phengite grain (Fig. 11), and indicate a decrease in the Rb/Sr ratio during exhumation. This implies that either Rb–Sr data from the unground phengite fractions are unreliable because of some artefact or, alternatively, that SIMS and EMP data from the single phengite grain are not representative of the whole population at the hand-specimen scale. However, several arguments support the conclusion that the major and trace element zoning detected in the single grain, at least in a relative sense, can be confidently assumed to be present in the other grains. First, spot data and X-ray maps show that major element zoning in the phengite grain analysed by SIMS is entirely comparable with that observed in other grains. Second, there is a simple explanation for the pronounced increase in Sr content toward the low-celadonite phengite rim, which would allow the extension of single grain observations to the whole phengite population: the inversion of aragonite to calcite during exhumation may have released significant amounts of Sr, such that the final stage of phengite chemical re-equilibration occurred in a Sr-rich system, as observed in other natural examples (Theye & Seidel, 1993). Even Rb–Sr data on fractions (2b) and (2c) are, therefore, inconsistent with the whole dataset and should be considered with great caution. This conclusion is corroborated by Rb–Sr data on the two splits [<0·10 mm (2d-1) and >0·25 mm (2d-2)] recovered after wet-grinding and sieving a fourth phengite fraction handpicked from the >0·50 mm grain size. Rb–Sr data from these two splits are very different (Table 3 and Fig. 11) and suggest the presence of calcite inclusions in the original untreated fraction. This implies that, although only inclusion-free phengite packets were handpicked, the unground fractions cannot be considered pure phengite separates. This observation does not demonstrate that Rb–Sr ages from untreated fractions (2a), (2b) and (2c) are meaningless, because the addition of calcite alone would move the composition of phengite toward the calcite end-member without changing the slope of the isochron line, but it does prove that the apparent negative correlation (at least for the Rb/Sr ratio) is an artefact caused by imperfect mineral separation. Additionally, given the large number of phengite grains in the analysed fractions, the heterogeneous Sr isotopic composition of the phengite fractions from the >0·50 mm grain size is probably due to contamination rather than to the presence of an older (pre-Alpine or prograde) radiogenic component. Another contaminant, besides calcite, could be an unidentified mineral phase(s) that has a high Sr content, a low Rb/Sr ratio and is enriched in ^{87}Sr with respect to phengite at the time of exhumation at upper crustal levels.

Mineral phases in the marble with these features are K-feldspar or epidote, and the hypothetical isotope composition could have been acquired by local isotope exchange during retrogression, as observed for minerals with low Rb/Sr ratios in other natural examples [e.g. matrix apatite and allanite of Meffan-Main *et al.* (2004)]. After all, even in sample CM1 the presence of excess Ar is certain, as ^{40}Ar–^{39}Ar ages significantly older (up to ~45–50 Ma) than the ~35 Ma UHP peak were also detected in areas most probably dominated by retrograde mantle phengites (i.e. in smaller grains or along the boundaries of millimetre-sized grains), for which the expected ages should instead fall within the 35–33 Ma interval. This statement is confirmed by the two ^{40}Ar–^{39}Ar *in situ* analyses on calcite, which, taking into account the volume sampled by the UV laser and normalizing Ar data to ~35 Ma, indicate that calcite contains approximately 10–15 ppb of parentless ^{40}Ar most probably hosted in fluid inclusions, thus supporting the interpretation that, at least at the time of aragonite inversion to calcite, grain boundary fluids still contained significant amounts of excess Ar. The above discussion leads us to conclude that Rb–Sr and ^{40}Ar–^{39}Ar data from impure marble CM1 are not internally consistent, and that Rb–Sr ages derived from all the unground phengite fractions, without the support of independent lines of evidence, should be considered unreliable. Among the six phengite fractions analysed for the Rb–Sr systematics, only wet-ground fractions (1) and (2d-2), yielding isochron ages of 36·45 ± 0·36 and 41·1 ± 0·40 Ma and preserving the age vs Rb/Sr ratio relationship (Fig. 11) defined by EMP–SIMS data, appear internally consistent. Taking into account the uncertainty in the ^{87}Rb decay constant, the Rb–Sr age from the smaller fraction (36·45 ± 0·62 Ma) overlaps within error with the estimated age for UHP conditions determined by means of U–Pb data; however, a straightforward comparison is hampered by the fact that the exact chemical composition of the analysed compositionally mixed phengite fraction remains unknown. The age from the larger fraction is instead significantly older, and even older than the Rb–Sr age from the eclogite. Regionally, considering that the larger-sized fraction is enriched in core phengites (as microchemical and ^{40}Ar–^{39}Ar data suggest) and assuming that a pure phengite fraction was analysed, the 41·1 ± 0·40-Ma age may speculatively represent a minimum estimate for the age of the prograde phengite relic.

Geochronological implications

^{40}Ar–^{39}Ar dating of UHP rocks

As discussed above, phengites from the different lithologies and amphibole from the eclogite are unquestionably plagued by excess Ar, and their ^{40}Ar–^{39}Ar ages are unreliable. Regionally, this is not a new finding. All phengite ages from previously published Ar data on the UHP–HP metamorphic rocks of the Dora Maira Massif, including those from the BIU (Monié & Chopin, 1991) and from the overlying HP units (Scaillet *et al.*, 1990, 1992), in light of the independently known *P–T–t* path for the BIU and of the results of more recent ^{40}Ar–^{39}Ar studies (Arnaud & Kelley, 1995; Hammerschmidt *et al.*, 1995; Monié & Bosch, 2000), are clearly unreliable because they are affected by excess Ar. The possible causes of inter-sample and intra-sample variations in Ar isotope compositions have been extensively discussed by Scaillet (1996, 1998) and will not be re-examined here. From a broad perspective, our results show that the complex intra-sample and inter-sample variations in Ar ages originated from superimposed factors and processes, namely, (1) age, composition and evolution of the protolith, and (2) dehydration vs hydration behaviour of the different lithologies during eclogitization and open- vs closed-system behaviour (i.e. availability of external aqueous fluids), which in turn determine the petrological evolution of the rock system and consequently of white mica. For example, phengites from the marble and eclogite, although mainly preserving major element compositions compatible with the UHP peak conditions and with only limited retrogression at upper crustal levels, contain markedly different concentrations of parentless ^{40}Ar (approximately 15 to 1·5 ppb and 80 to 30 ppb for marble and eclogite, respectively). This observation indicates initial differences in the concentration of excess Ar in the grain boundary network and suggests that excess Ar was internally derived. Furthermore, in all studied phengites *in situ* Ar laserprobe data reveal a complex within-sample intra-grain and inter-grain spatial distribution of apparent ^{40}Ar–^{39}Ar ages, which is closely linked to microchemical and microtextural variations. Most of the millimetre-sized grains from the three lithologies exhibit a well-defined core–rim relationship, with Ar ages decreasing from the core to grain boundaries. Such an evolution, along with microchemical data, parallels the results of other studies (e.g. Giorgis *et al.*, 2000) but contrasts with other works in which age gradients are consistent with a late influx of excess Ar into the mineral grain boundaries (i.e. increasing ages from core to rim; e.g. Pickles *et al.*, 1997; Sherlock *et al.*, 1999; Sherlock & Kelley, 2002). This evolution is compatible with concentrations of excess Ar in the grain boundary network decreasing with time during exhumation [e.g. by incorporation of excess Ar in minerals from a finite reservoir (Arnaud & Kelley, 1995)], and/or with the decreasing salinity of grain boundary fluids as a result of local changes in the mineral–fluid equilibria or, less likely, because of the introduction of external aqueous fluids. High concentrations of parentless ^{40}Ar in the grain boundary network, however, must have persisted in all

studied samples during exhumation at upper crustal levels, as evidenced in the eclogite by the geologically meaningless amphibole ages and in the marble by the excess Ar detected in calcite. It should be noted that the strong compositional control on excess Ar concentrations in phengite grains precludes a straightforward evaluation of the length scale of Ar isotope equilibrium (i.e. whether at the grain scale or at the hand-specimen scale), because it requires the chemical characterization of the exact volume sampled by the laserprobe during *in situ* analysis.

It should be noted that the presence of excess Ar does not preclude considerations on Ar retentivity in phengite. The preservation of Ar concentration gradients at the grain scale indicates that the Ar isotope signature pertaining to different metamorphic stages survived in phengite, even though most of the decompressional path of the studied samples occurred at temperatures exceeding 600°C (see Giorgis *et al.*, 2000; Di Vincenzo *et al.*, 2001). This shows the strong potential of the *in situ* ^{40}Ar–^{39}Ar laser technique applied to white mica, coupled with microtextural and microchemical characterization, in resolving discrete *P*–*T*–deformation stages under UHP–HP regimes, provided that mineral contamination by excess Ar is demonstrably a negligible factor. According to the above arguments, young protoliths with low K contents and prevailing dehydration behaviour along the prograde path certainly represent the best candidates to fully exploit this potential (Foland, 1979; Scaillet, 1996, 1998; Kelley, 2000). However, even in young protoliths the presence of only cryptic evidence of excess Ar in some cases (e.g. Sherlock & Kelley, 2002) may require the use of compositionally different rock samples and the support of independent temporal constraints.

Lastly, a common feature to all age spectra from step-heating analysis is that they are internally discordant, and those from the impure marble and the orthogneiss show reproducible patterns with a typical hump shape and increasing ages at high temperatures. This feature is not surprising, because the studied phengites consist of coexisting heterochemical white micas, which release Ar upon heating over different temperature ranges (Wijbrans & McDougall, 1986; Sletten & Onstott, 1998; Tomaschek *et al.*, 2003). However, the true age interval preserved in the chemically heterogeneous phengites and revealed by *in situ* dating is only at best approached by the step ages from step-heating analysis. Although chemical data from neutron-produced Ar isotopes indicate that pure phengite was analysed, $^{37}Ar_{Ca}$ and $^{38}Ar_{Cl}$ intensities close to the detection limits are unfortunately of limited use in determining pure end-members from three-isotope correlation plots, as has been determined in other studies (e.g. Villa *et al.*, 2000; Tomaschek *et al.*, 2003).

Rb–Sr dating of UHP rocks

Results from the present study confirm the potential, recently demonstrated by Glodny *et al.* (2002, 2003, 2005), of phengite-based Rb–Sr internal mineral isochrons in determining the precise crystallization ages of eclogite-facies mineral assemblages. Interestingly, the physical conditions experienced by our samples during eclogitization were even more severe than those experienced by rock samples investigated by Glodny *et al.* (2002, 2003, 2005). Furthermore, Rb–Sr phengite ages, compatible with timing of the UHP metamorphic stage, were obtained not only for a metabasite, in which phengite had as potential main exchange partners for Sr isotopes omphacite and garnet (both characterized by slow diffusion kinetics; Dahl, 1997), but also for the marble, in which the dominant exchange partners were carbonates, with significantly higher expected diffusivities (e.g. for calcite, Cherniak, 1997). Besides major element zoning, the phengite from marble CM1 also preserves a pronounced zoning of trace elements (including Rb and Sr). It should be noted that chemical diffusion data are commonly applied to problems of isotope exchange (Ganguly & Ruiz, 1987; Cherniak & Watson, 1994), and that the closure temperature concept (Dodson, 1973) assumes homogeneous and temporally constant parent and daughter concentrations across the grain (see Jenkin *et al.*, 2001). An important implication of the within-grain elemental zoning of both Rb–Sr and major elements in white mica is that microchemical data on major elements (e.g. by EMP) and trace elements [e.g. determined by SIMS or PIXE (particle-induced X-ray emission)] may be used to establish a qualitative or quantitative link (depending on how representative the investigated single grains are of the whole mineral population at the hand-specimen scale) between petrology and Sr isotope records.

A final question to be addressed concerns the effect of parent–daughter zoning across phengite grains when comparing Rb–Sr with ^{40}Ar–^{39}Ar results from metamorphic rocks that behaved as a closed system in which temperature was not the limiting factor controlling the rate of isotope transport (e.g. UHP and HP rocks). In many natural examples ^{40}Ar–^{39}Ar ages from white mica are found to be significantly older or younger than white mica-based Rb–Sr isochron ages derived from the same sample. This phenomenon is commonly attributed *a priori* to the presence of excess Ar or is considered to conform to the age sequence muscovite Rb–Sr > muscovite K–Ar. Although the first possibility also applies to the studied samples, the pronounced Rb and Sr zoning, coupled with negligible variations in K, suggests that the two interpretations may not hold true in some cases. The results from the marble illustrate that phengite at the grain scale exhibits negligible variations in K contents, although

both Rb and Sr vary significantly (Rb/Sr ratio from ~500 to ~40 from the core to the rim). This implies that the K–Ar age will reflect the actual proportions by weight of the diachronous white micas composing the grain, whereas the Rb–Sr age will also be influenced by Rb and Sr variations across the grain and by the Rb and Sr contents of the matrix with which white mica originally exchanged Sr isotopes. In a rock system such as a marble, in which white mica predominantly equilibrated with a matrix characterized by a very low Rb/Sr ratio and a nearly constant isotope ratio in time, any difference between Rb–Sr ages and K–Ar ages will mainly be dictated by variations in Rb contents at the grain scale, with Rb–Sr ages that are older or younger than K–Ar ages, depending on whether the Rb content decreases or increases from the core to the rim. A similar decoupling was recently used by Lapen *et al.* (2003) to explain the apparent inconsistency between Lu–Hf and Sm–Nd garnet ages from the same eclogite sample, which were found to differ by as much as $8{\cdot}2 \pm 3{\cdot}3$ Ma. The different core-to-rim variations in Lu, Hf, Sm and Nd lead the Lu–Hf age to be weighted toward the older garnet core relative to the Sm–Nd age, which is thought to reflect later garnet growth instead. Such a potential decoupling between Rb–Sr and K–Ar systems, however, obviously becomes negligible when the tectonometamorphic evolution of a metamorphic terrain occurred in a short time interval (i.e. a few million years), such that inherent differences in age are lost within analytical uncertainties.

ACKNOWLEDGEMENTS

G.D.V. is grateful to F. Olmi for support during EMP analysis at the IGG–CNR (Firenze). D.C. and B.L. thank A. Alberico, P. Cadoppi and C. Groppo for help with EDS microanalysis at the IGG–CNR (Torino). Careful and constructive reviews by P. S. Dahl, J. Glodny and I. M. Villa are gratefully acknowledged. Research was funded by the CNR. The Ar laserprobe facility was funded by the Programma Nazionale di Ricerche in Antartide (PNRA), and instrumental maintenance was ensured by CNR.

SUPPLEMENTARY DATA

Supplementary data for this paper are available at *Journal of Petrology* online.

REFERENCES

Agard, P., Monié, P., Jolivet, L & Goffé, B. (2002). Exhumation of the Schistes Lustrés complex: *in situ* laser probe $^{40}Ar/^{39}Ar$ constraints and implications for the Western Alps. *Journal of Metamorphic Geology* **20**, 599–618.

Arnaud, N. O. & Kelley, S. P. (1995). Evidence for excess Ar during high pressure metamorphism in the Dora Maira Massif (western Alps, Italy), using an ultra-violet laser ablation microprobe ^{40}Ar–^{39}Ar technique. *Contributions to Mineralogy and Petrology* **121**, 1–11.

Baksi, A. K., Archimbald, D. A. & Farrar, E. (1996). Intercalibration of $^{40}Ar/^{39}Ar$ dating standards. *Chemical Geology* **129**, 307–324.

Begemann, F., Ludwig, K. R., Lugmair, G. W., Min, K., Nyquist, L. E., Patchett, P. J., Renne, P. J., Shih, C.-Y., Villa, I. M. & Walker, R. J. (2001). Call for improved set of decay constants for geochronological use. *Geochimica et Cosmochimica Acta* **65**, 111–121.

Biino, G. & Compagnoni, R. (1991). Very-high pressure metamorphism of the Brossasco coronite metagranite, southern Dora Maira Massif, Western Alps. *Schweizerische Mineralogische und Petrographische Mitteilungen* **72**, 347–363.

Castelli, D., Compagnoni, R. & Rolfo, F. (2004). UHP impure marble from the Brossasco–Isasca unit (Dora-Maira Massif, western Alps): further evidence for alpine recrystallization within the diamond stability field. *32nd IGC, Florence 2004, Abstracts*.

Cherniak, D. J. (1997). An experimental study of strontium and lead diffusion in calcite, and implications for carbonate diagenesis and metamorphism. *Geochimica et Cosmochimica Acta* **61**, 4173–4179.

Cherniak, D. J. & Watson, B. (1994). A study of strontium diffusion in plagioclase using Rutherford backscattering spectroscopy. *Geochimica et Cosmochimica Acta* **58**, 5179–5190.

Chopin, C. (1984). Coesite and pure pyrope in high-grade blueschists of the western Alps: a first record and some consequences. *Contributions to Mineralogy and Petrology* **86**, 107–118.

Chopin, C. (2003). Ultrahigh-pressure metamorphism: tracing continental crust into the mantle. *Earth and Planetary Science Letters* **212**, 1–14.

Chopin, C. & Schertl, H.-P. (1999). The UHP Unit in the Dora-Maira Massif, Western Alps. *International Geology Review* **41**,765–780.

Chopin, C., Henry, C. & Michard, A. (1991). Geology and petrology of the coesite-bearing terrain, Dora-Maira massif, Western Alps. *European Journal of Mineralogy* **3**, 263–329.

Compagnoni, R. & Hirajima, T. (2001). Superzoned garnets in the coesite-bearing Brossasco–Isasca Unit, Dora-Maira massif, Western Alps, and the origin of the whiteschists. *Lithos* **57**, 219–236.

Compagnoni, R. & Rolfo, F. (2003). UHPM units in the Western Alps. In: Carswell, D. A. & Compagnoni, R. (eds) *Ultrahigh Pressure Metamorphism. EMU Notes in Mineralogy* **5**, 13–50.

Compagnoni, R., Hirajima, T. & Chopin, C. (1995). Ultra-high-pressure metamorphic rocks in the Western Alps. In: Coleman, R. G. & Wang, X. (eds) *Ultrahigh Pressure Metamorphism*. Cambridge: Cambridge University Press, pp. 206–243.

Dahl, P. S. (1996). The crystal–chemical basis for Ar retention in micas: inferences from interlayer partitioning and implications for geochronology. *Contributions to Mineralogy and Petrology* **123**, 22–39.

Dahl, P. S. (1997). A crystal-chemical basis for Pb retention and fission-track annealing systematics in U-bearing minerals, with implications for geochronology. *Earth and Planetary Science Letters* **150**, 277–290.

Dahl, P. S. & Frei, R. (1998). Step-leach Pb–Pb dating of inclusion-bearing garnet and staurolite, with implications for Early Proterozoic tectonism in the Black Hills collisional orogen, South Dakota, United States. *Geology* **26**, 111–114.

Di Vincenzo, G. & Palmeri, R. (2001). An ^{40}Ar–^{39}Ar investigation of high–pressure metamorphism and the retrogressive history of mafic eclogite from the Lanterman Range (Antarctica): evidence against a simple temperature control on Ar transport in amphibole. *Contributions to Mineralogy and Petrology* **141**, 15–35.

Di Vincenzo, G., Ghiribelli, B., Giorgetti, G. & Palmeri, R. (2001). Evidence of a close link between petrology and isotope records: constraints from SEM, EMP, TEM and *in situ* ^{40}Ar–^{39}Ar laser

analyses on multiple generations of white micas (Lanterman Range, Antarctica). *Earth and Planetary Science Letters* **192**, 389–405.

Di Vincenzo, G., Viti, C. & Rocchi, R. (2003). The effect of chlorite interlayering on ^{40}Ar–^{39}Ar biotite dating: an ^{40}Ar–^{39}Ar laserprobe and TEM investigation of variably chloritised biotites. *Contributions to Mineralogy and Petrology* **145**, 643–658.

Di Vincenzo, G., Carosi, R. & Palmeri, R. (2004). The relationship between tectono-metamorphic evolution and Ar isotope records in white mica: constraints from *in situ* ^{40}Ar–^{39}Ar laser analysis of the Variscan basement of Sardinia (Italy). *Journal of Petrology* **45**, 1013–1043.

Dodson, M. H. (1973). Closure temperature in cooling geochronological and petrological systems. *Contributions to Mineralogy and Petrology* **40**, 259–274.

Duchêne, S., Blichert-Toft, J., Luais, B., Télouk, P., Lardeaux, J.-M. & Albarède, F. (1997). The Lu–Hf dating of garnets of the Alpine high-pressure metamorphism. *Nature* **387**, 586–589.

Ferraris, C., Castelli, D. & Lombardo, B. (2005). SEM/TEM–AEM characterization of micro- and nano-scale zonation in phengite from a UHP Dora-Maira marble: significance of armoured Si-rich domains and some petrologic implications. *European Journal of Mineralogy* **17**, 453–464.

Foland, K. A. (1979). Limited mobility of Ar in a metamorphic terrane. *Geochimica et Cosmochimica Acta* **43**, 793–801.

Ganguly, J. & Ruiz, J. (1987). Time–temperature relation of mineral isochrons: a thermodynamical model, and illustrative examples for the Rb–Sr system. *Earth and Planetary Science Letters* **81**, 338–348.

Gebauer, D., Schertl, H.-P., Brix, M. & Schreyer, W. (1997). 35 Ma old ultrahigh-pressure metamorphism and evidence for very rapid exhumation in the Dora Maira Massif, Western Alps. *Lithos* **41**, 5–24.

Giorgis, D., Cosca, M. & Li, S. (2000). Distribution and significance of extraneous Ar in UHP eclogite (Sulu terrain, China): insight from *in situ* ^{40}Ar/^{39}Ar UV–laser ablation analysis. *Earth and Planetary Science Letters* **181**, 605–615.

Glodny, J., Bingen, B., Austrheim, H., Molina, J. F. & Rusin, A. (2002). Precise eclogitization ages deduced from Rb/Sr mineral system: the Maksyutov complex, southern Urals, Russia. *Geochimica et Cosmochimica Acta* **66**, 1221–1235.

Glodny, J., Austrheim, H., Molina, J. F., Rusin, A. & Steward, D. (2003). Rb/Sr record of fluid–rock interaction in eclogites: the Marun-Keu complex, Polar Urals, Russia. *Geochimica et Cosmochimica Acta* **67**, 4353–4371.

Glodny, J., Ring, U., Kühn, A., Gleissner, P. & Franz, G. (2005). Crystallization and very rapid exhumation of the youngest alpine eclogites (Tauern Window, Eastern Alps) from Rb/Sr mineral assemblage analysis. *Contributions to Mineralogy and Petrology* **149**, 699–712.

Gray, D. R., Hand, M., Mawby, J., Armstrong, R. A., Miller, J. Mc. L. & Gregory, R. T. (2004). Sm–Nd and zircon U–Pb ages from garnet-bearing eclogites, NE Oman: constraints on high-*P* metamorphism. *Earth and Planetary Science Letters* **222**, 407–422.

Groppo, C., Lombardo B., Castelli, D. & Cadoppi, P. (2005). Decompressional *P–T* path in the albite-stability field of orthogneiss from the UHP unit of the Dora-Maira Massif (western Alps). *7th International Eclogite Conference, Graz, 3–9 July, Abstracts*.

Groppo, C., Castelli, D. & Compagnoni, R. (2006). Late chloritoid–staurolite assemblage in a garnet–kyanite-bearing metapelite from the ultrahigh-pressure Brossasco–Isasca unit (Dora-Maira Massif, Western Alps): new petrological constraints for a portion of the decompressional path. In: Hacker, B. R., McClelland, W. C. & Liou, J. G. (eds) *Ultrahigh-pressure Metamorphism: Deep Continental Subduction. Geological Society of America, Special Papers* **403**, 127–138.

Hacker, B. R., Ratschbacher, L., Webb, L., Ireland, T., Walker, D. & Shuwen, D. (1998). U/Pb zircon ages constrain the architecture of the ultrahigh-pressure Qinling–Dabie Orogen, China. *Earth and Planetary Science Letters* **215**, 215–230.

Hames, W. E. & Cheney, J. T. (1997). On the loss of ^{40}Ar* from muscovite during polymetamorphism. *Geochimica et Cosmochimica Acta* **61**, 3863–3872.

Hammerschmidt, K. & Frank, E. (1991). Relicts of high pressure metamorphism in the Lepontine Alps (Switzerland)—^{40}Ar/^{39}Ar and microprobe analyses on white micas. *Schweizerische Mineralogische und Petrographische Mitteilungen* **71**, 261–264.

Hammerschmidt, K., Schertl, H. P., Friedrichsen, H. & Schreyer, W. (1995). Excess Ar a common feature in ultrahigh-pressure rocks: a case study on micas from the Dora-Maira Massif, western Alps, Italy. *Terra Nova* **7**, 349.

Hermann, J. (2003). Experimental evidence for diamond-facies metamorphism in the Dora-Maira massif. *Lithos* **70**, 163–182.

Holland, T. J. B. & Powell, R. (1998). An internally consistent thermodynamic data set of petrological interest. *Journal of Metamorphic Geology* **16**, 309–343.

Jenkin, G. R., Ellan, R. M., Rogers, G. & Stuart, F. M. (2001). An investigation of closure temperature of the biotite Rb–Sr system: the importance of cation exchange. *Geochimica et Cosmochimica Acta* **65**, 1141–1160.

Kelley, S. P. (2002). Excess Ar in K–Ar and Ar–Ar geochronology. *Chemical Geology* **188**, 1–22.

Kelley, S. P. & Wartho, J.-A. (2000). Rapid ascent and the significance of Ar–Ar ages in xenolith phlogopites. *Science* **289**, 609–611.

Kienast, J. R., Lombardo, B., Biino, G. & Pinardon, J. L. (1991). Petrology of very high-pressure eclogitic rocks from the Brossasco–Isasca Complex, Dora-Maira Massif, Italian western Alps. *Journal of Metamorphic Geology* **9**, 19–34.

Kühn, A., Glodny, J., Iden, K. & Austrheim, H. (2000). Retention of Precambrian Rb/Sr phlogopite ages through Caledonian eclogite facies metamorphism, Bergen Arc Complex, W Norway. *Lithos* **51**, 305–330.

Lanphere, M. A. & Darlymple, G. B. (1976). Identification of excess ^{40}Ar by the ^{40}Ar/^{39}Ar age spectrum technique. *Earth and Planetary Science Letters* **32**, 141–148.

Lapen, T. J., Johnson, C. M., Baumgartner, L. P., Mahlen, N. J., Beard, B. L. & Amato, J. M. (2003). Burial rates during prograde metamorphism of an ultra-high-pressure terrane: an example from Lago di Cignana, western Alps, Italy. *Earth and Planetary Science Letters* **215**, 57–72.

Leake, B. E., Woolley, A. R., Arps, C. E. S., Birch, W. D., Gilbert, M. C., Grice, J. D. *et al.* (1997). Nomenclature of amphiboles: report of the subcommittee on amphiboles of the International Mineralogical Association, commission on new minerals and mineral names. *Canadian Mineralogist* **35**, 219–246.

Li, S., Wang, S., Chen, Y., Liu, D., Qiu, J., Zhou, H. & Zhang, Z. (1994). Excess Ar in phengite from eclogite: evidence from dating of eclogitic minerals by Sm–Nd, Rb–Sr and ^{40}Ar/^{39}Ar methods. *Chemical Geology* **112**, 343–350.

Ludwig, K. R. (2003). User's manual for Isoplot/Ex version 3.00, a geochronological toolkit for Microsoft Excel. *Berkeley Geochronology Center Special Publications* **4**, 72 pp.

Massonne, H. J. & Schreyer, W. (1987). Phengite geobarometry based on the limiting assemblage with K-feldspar, phlogopite and quartz. *Contributions to Mineralogy and Petrology* **96**, 212–224.

Maurel, O., Monié, P., Resput, J. P., Leyreloup, A. F. & Maluski, H. (2003). Pre-metamorphic ^{40}Ar/^{39}Ar and U–Pb age in HP metagranitoids from the Hercynian belt (France). *Chemical Geology* **193**, 195–214.

Meffan-Main, S., Cliff, R. A., Barnicoat, A. C., Lombardo, B. & Compagnoni, R. (2004). A Tertiary age for Alpine high-pressure

metamorphism in the Gran Paradiso massif: a Rb–Sr microsampling study. *Journal of Metamorphic Geology* **22**, 267–281.

Michard, A., Henry, C. & Chopin, C. (1995). Structures in ultrahigh-pressure metamorphic rocks. In: Coleman, R. G. & Wang, X. (eds) *Ultrahigh Pressure Metamorphism*. Cambridge: Cambridge University Press, pp. 132–158.

Monié, P. & Bosch, D. (2000). Nouvelles données géochronologiques $^{40}Ar/^{39}Ar$, Rb–Sr et Sm–Nd sur les éclogites du Monviso et de Dora Maira (Alpes Occidentales). *Réunion Annuelle des Sciences de la Terre, Abstracts*, p. 198.

Monié, P. & Chopin, C. (1991). $^{40}Ar/^{39}Ar$ dating in coesite-bearing and associated units of the Dora Maira massif, Western Alps. *European Journal of Mineralogy* **3**, 239–262.

Nowlan, E. U., Schertl, H. P. & Schreyer, W. (2000). Garnet–omphacite–phengite thermobarometry of eclogites from the coesite-bearing unit of the southern Dora Maira Massif, Western Alps. *Lithos* **52**, 197–214.

Ottolini, L., Camara, F. & Devouard, B. (2004). New SIMS procedures for the characterization of a complex silicate matrix, Na_3(REE,Th, Ca,U)$Si_6O_{15}\cdot 2{\cdot}5H_2O$ (Sazhinite), and comparison with EMPA and SREF results. *Microchimica Acta* **145**, 139–146.

Paquette, J.-L., Chopin, C. & Peucat, J.-J. (1989). U–Pb zircon, Rb–Sr and Sm–Nd geochronology of high- to very-high-pressure meta-acidic rocks from western Alps. *Contributions to Mineralogy and Petrology* **101**, 280–289.

Philippot, P., Chevallier, P., Chopin, C. & Dubessy, J. (1995). Fluid composition and evolution in coesite-bearing rocks (Dora-Maira massif, western Alps): implications for element recycling during subduction. *Contributions to Mineralogy and Petrology* **121**, 29–44.

Philippot, P. & Rumble, D. (2000). Fluid–rock interactions during high-pressure and ultrahigh-pressure metamorphism. *International Geology Review* **42**, 312–327.

Pickles, C. S., Kelley, S. P., Reddy, S. M. & Wheeler, J. (1997). Determinations of high spatial resolution Ar isotope variations in metamorphic biotites, *Geochimica et Cosmochimica Acta* **61**, 3809–3833.

Proyer, A. (2003). The preservation of high-pressure rocks during exhumation: metagranites and metapelites. *Lithos* **70**, 183–194.

Ravna, E. J. K. & Terry, M. P. (2004). Geothermobarometry of UHP and HP eclogites and schists—an evaluation of equilibria among garnet–clinopyroxene–kyanite–phengite–coesite/quartz. *Journal of Metamorphic Geology* **22**, 579–592.

Romer, R. L. (2001). Lead incorporation during crystal growth and the misinterpretation of geochronological data from low-$^{238}U/^{204}Pb$ metamorphic minerals. *Terra Nova* **13**, 258–263.

Rubatto, D. & Gebauer, D. (2000). Use of cathodoluminescence for U–Pb zircon dating by ion microprobe: some examples from the Western Alps. In: Pagel, M., Barbin, V., Blanc, Ph. & Ohnenstetter, D. (eds) *Cathodoluminescence in Geosciences*. Berlin: Springer, pp. 373–400.

Rubatto, D. & Hermann, J. (2001). Exhumation as fast as subduction? *Geology* **29**, 3–6.

Ruffet, G., Gruau, G., Ballèvre, M., Féraud, G. & Philippot, P. (1997). Rb–Sr and ^{40}Ar–^{39}Ar laser probe dating of high-pressure phengites from the Sesia zone (Western Alps): underscoring of excess Ar and new constraints on the high-pressure metamorphism. *Chemical Geology* **141**, 1–18.

Scaillet, S. (1996). Excess ^{40}Ar transport scale and mechanism in the high-pressure phengites: a case study from an eclogitized metabasite of the Dora-Maira nappe, western Alps. *Geochimica et Cosmochimica Acta* **60**, 1075–1090.

Scaillet, S. (1998). K–Ar ($^{40}Ar/^{39}Ar$) geochronology of ultrahigh pressure rocks. In: Hacker, B. R. & Liou, J. G. (eds) *When Continents Collide: Geodynamics and Geochemistry of Ultrahigh-Pressure Rocks*. Dordrecht: Kluwer Academic, pp. 161–201.

Scaillet, S., Féraud, G., Lagabrielle, Y., Ballèvre, M. & Ruffet, G. (1990). $^{40}Ar/^{39}Ar$ laser-probe dating by step-heating and spot-fusion of phengites from the Dora Maira nappe of the western Alps, Italy. *Geology* **18**, 741–744.

Scaillet, S., Féraud, G., Ballèvre, M. & Amouric, M. (1992). Mg/Fe and [(Mg,Fe)Si–Al_2] compositional control on Ar behaviour in high-pressure white micas: a $^{40}Ar/^{39}Ar$ continuous laser-probe study from the Dora-Maira nappe of the internal western Alps, Italy. *Geochimica et Cosmochimica Acta* **56**, 2851–2872.

Schertl, H. P., Schreyer, W. & Chopin, C. (1991).The pyrope–coesite rocks and their country rocks at Parigi, Dora Maira massif, western Alps: detailed petrography, mineral chemistry and *PT*-path. *Contributions to Mineralogy and Petrology* **108**, 1–21.

Schmidt, M. W. (1993). Phase relations and compositions in tonalite as a function of pressure: an experimental study at 650°C. *American Journal of Science* **293**, 1011–1060.

Sharp, Z. D., Essene, E. J. & Hunziker, J. C. (1993). Stable isotope geochemistry and phase equilibria of coesite-whiteschists, Dora Maira Massif, Western Alps. *Contributions to Mineralogy and Petrology* **114**, 1–12.

Sherlock, S. & Kelley, S. P. (2002). Excess Ar evolution in HP–LT rocks: a UVLAMP study of phengite and K-free minerals, NW Turkey. *Chemical Geology* **182**, 619–636.

Sherlock, S., Kelley, S. P., Inger, S., Harris, N. & Okay, A. (1999). $^{40}Ar/^{39}Ar$ and Rb–Sr geochronology of high-pressure metamorphism and exhumation history of the Tavsanli Zone, NW Turkey. *Contributions to Mineralogy and Petrology* **137**, 46–58.

Sletten, V. W. & Onstott, T. C. (1998). The effect of the instability of muscovite during *in vacuo* heating on $^{40}Ar/^{39}Ar$ step-heating spectra. *Geochimica et Cosmochimica Acta* **62**, 123–141.

Theye, T. & Seidel, E. (1993). Uplift-related retrogression history of aragonite marbles in Western Crete (Greece). *Contributions to Mineralogy and Petrology* **114**, 349–356.

Tilton, G. R., Schreyer, W. & Schertl, H.-P. (1989). Pb–Sr–Nd isotopic behaviour of deeply subducted crustal rocks from the Dora Maira massif, Western Alps Italy. *Geochimica et Cosmochimica Acta* **53**, 1391–1400.

Tilton, G. R., Schreyer, W. & Schertl, H.-P. (1991). Pb–Sr–Nd isotopic behaviour of deeply subducted crustal rocks from the Dora Maira massif, Western Alps Italy—II: what is the age of the ultrahigh-pressure metamorphism? *Contributions to Mineralogy and Petrology* **108**, 22–33.

Tomaschek, F., Kennedy, A. K., Villa, I. M., Lagos, M. & Ballhaus, C. (2003). Zircon from Syros, Cyclades, Greece—recrystallization and mobilization of zircon during high-pressure metamorphism. *Journal of Petrology* **44**, 1977–2002.

Tonarini, S., Villa, I. M., Oberli, F., Meier, M., Spencer, D., Pognante, U. & Ramsay, J. G. (1993). Eocene age of eclogite metamorphism in Pakistan Himalaya: implication for India–Eurasia collision. *Terra Nova* **5**, 13–20.

Verschure, R. H., Andriessen, P. A. M., Boelrijk, N. A. I. M., Hebeda, E. H., Maijer, C., Priem, H. N. A. & Verdurmen, E. A. Th. (1980). On the thermal stability of Rb–Sr and K–Ar biotite systems: evidence from coexisting Sveconorwegian (*ca.* 870 Ma) and Caledonian (*ca.* 400 Ma) biotites in SW Norway. *Contributions to Mineralogy and Petrology* **74**, 245–252.

Villa, I. M. (1998). Isotopic closure. *Terra Nova* **10**, 42–47.

Villa, I. M., Hermann, J., Müntener, O. & Trommsdorff, V. (2000). ^{39}Ar–^{40}Ar dating of multiply zoned amphibole generations (Malenco, Italian Alps). *Contributions to Mineralogy and Petrology* **140**, 363–381.

Wijbrans, J. R. & McDougall, I. (1986). $^{40}Ar/^{39}Ar$ dating of white micas from an Alpine high-pressure metamorphic belt on Naxos (Greece): the resetting of the Ar isotopic system. *Contributions to Mineralogy and Petrology* **93**, 187–194.

APPENDIX: ANALYTICAL TECHNIQUES

Mineral analyses on polished thin sections (samples CM1, BR2, D1 and D2) and on representative phengite concentrates (see below) of samples CM1 and BR2 mounted with epoxy resin were carried out using a Cambridge S-360 scanning electron microscope (SEM) equipped with a LINK-EDS-860 X-ray energy dispersive system (EDS) at IGG–CNR Torino. Representative mineral analyses are shown in Table 1. Accelerating voltage was 15 kV and the sample current 0·5 nA. Natural standards were used for calibration. Precision and accuracy, and the procedure used for qualitative elemental X-ray maps have been given by Ferraris *et al.* (2005).

Trace elements in phengite [grain (3)] from impure marble CM1 mounted with epoxy resin were analysed by secondary ion mass spectrometry (SIMS) with a Cameca IMS 4f ion microprobe at IGG–CNR Pavia. An energy filtering technique (75–125 eV secondary ions) was applied to remove molecular ion interferences. Secondary ions were extracted and focused under an ion-image field of 25 μm, and contrast diaphragm and field aperture of 400 and 1800 μm diameter, respectively, at a mass resolution of ~600 ($M/\Delta M$). Analyses were performed on a Pt-coated section with a 12·5 kV accelerated $^{16}O^-$ primary beam at 3 nA current intensity and spot size of ~5 μm diameter. Signals from the following isotopes were detected: $^{7}Li^+$, $^{9}Be^+$, $^{11}B^+$, $^{19}F^+$, $^{45}Sc^+$, $^{47}Ti^+$, $^{51}V^+$, $^{52}Cr^+$, $^{85}Rb^+$, $^{88}Sr^+$, $^{90}Zr^+$, $^{93}Nb^+$, $^{133}Cs^+$, $^{138}Ba^+$ and ^{30}Si (as the inner reference for the matrix). Ion signals were acquired in two analytical sessions. We analysed Sr only in the first session, and all the above-listed trace elements in the second session. Quantification of ion signals was carried out by means of the empirical approach of relative sensitivity factors (RSFs), which were derived from international standards and well-characterized reference materials (kaersutite Soda Springs, BB, BCR-2G, JDF-D2 glasses and Kakanui augite). Accuracy is in the range of 5–10% for Li, Be, B, Sc, Ti, V and Zr; ~10% for Sr and Ba; and ~15% for Cr and Rb. SIMS data for Cr at 2 ppm concentration are close to our detection limit. Further details on SIMS analysis have been given by Ottolini *et al.* (2004). Major element concentrations were determined at IGG–CNR Firenze using a JEOL JX 8600 electron microprobe (EMP) fitted with four wavelength-dispersive spectrometers close to each SIMS spot, and the corresponding SiO_2 (wt %) contents were used in the calculation of SIMS data (Table 2). Cl was below the detection limit (<100 ppm) in all EMP measurements.

Mineral separation and ^{40}Ar–^{39}Ar and Rb–Sr analysis were carried out at IGG–CNR Pisa. Samples were crushed and sieved, and standard separation techniques were used to concentrate the 0·16–0·25 mm grain fraction. After further manual purification under a binocular microscope, the concentrates were cleaned ultrasonically with deionized water and methanol. White mica concentrates from the 0·16–0·25 mm grain size were ground for a few minutes in deionized water using an agate mortar and pestle grinder and then sieved again (>0·16 mm) to obtain inclusion-free separates. In addition, single white-mica grains were handpicked from the >0·50 mm grain fraction and cleaned as above. Rock chips 8·5 mm in diameter were drilled from double-polished sections (~300 μm thick) and ultrasonically cleaned in deionized water and methanol. Samples were wrapped in aluminium foil and irradiated for 20 h, along with the FCT-3 biotite standard (27·95 Ma; Baksi *et al.* 1996), in the TRIGA reactor at the University of Pavia (Italy). ^{40}Ar–^{39}Ar laser analyses were performed using the IR laser step-heating technique on both mineral fractions and single grains. The IR and UV *in situ* techniques were used both perpendicular to the cleavage plane of single phengite grains and parallel to the basal cleavage of phengites in the rock chips. After irradiation, samples were placed in an ultrahigh-vacuum laser port and baked overnight at about 180°C. *In situ* laser ^{40}Ar–^{39}Ar determinations were carried out using a single-mode laser beam generated by a continuous wave diode-pumped Nd:YAG (Nd-doped yttrium–aluminium–garnet) IR laser (maximum power 20 W) connected to an external computer-controlled shutter and a pulsed Nd:YAG UV laser (frequency quadrupled and Q-switched). The size of the sampled volume was selected to obtain analytical errors better than ±3–4% (2σ). Single IR laser shots (lasting 20–30 ms) of the IR laser (operating at ~15 W) were focused to producing melt pits ~150 μm in diameter. Multiple (2–3) shorter pulses (10 ms) at a lower laser power (10–12 W) were instead used along the rim of crystals or for smaller flakes. The UV laser, operating at 20 Hz and 0·5–1 mJ per pulse, was focused to ~10 μm and repeatedly rastered by a computer-controlled *x*–*y* stage over areas of ~100 × 200 μm^2 to produce pits 50–100 μm deep. The sample was observed by a CCD camera coaxial with the laser beam. For step-heating analyses, the IR laser beam was defocused to a ~2 mm spot size and homogenized by a beam-homogenizer lens, which produces a flat power distribution. A total of ~5 mg of amphibole, ~50 white mica flakes of the 0·16–0·25 mm fraction for sample BR2, and ~100 flakes of the 0·16–0·25 mm fraction for sample CM1 were loaded into the 3 mm diameter holes of a copper palette holder, and homogeneous heating was obtained by slowly

rastering the laser beam. Single white mica grains from the >0·50 mm grain fraction of samples BR2, CM1 and D1, and single biotite grains from samples D1 and D2 were instead laser heated at a fixed position. Steps were carried out at increasing laser power until complete melting occurred. After cleanup (10 and 20 min for *in situ* IR and UV analysis, respectively, and 10–12 min for IR incremental laser heating analysis), extracted gases were equilibrated via automated valves into a MAP215-50 mass spectrometer fitted with a Balzers SEV217 secondary electron multiplier. Ar isotope peak intensities were measured 10 times for a total of ~20 min. Blanks were analysed every two to four analyses. Data corrected for post-irradiation decay, mass discrimination effects, isotopes derived from interfering neutron reactions, and blanks are listed in Tables A and B, available as supplementary material on the *Journal of Petrology* web site. Errors are 2σ and do not include the uncertainty in the J value (analytical error), which was included in the total gas ages and the weighted mean ages. The interference factors, determined on phases of K and Ca were: $(^{40}Ar/^{39}Ar)_K$ = 0·0084, $(^{38}Ar/^{39}Ar)_K$ = 0·013, $(^{36}Ar/^{37}Ar)_{Ca}$ = 0·00024 and $(^{39}Ar/^{37}Ar)_{Ca}$ = 0·00075. The K/Ca and K/Cl ratios can be derived by multiplying $^{39}Ar_K/^{37}Ar_{Ca}$ and $^{39}Ar_K/^{38}Ar_{Cl}$ by 0·53 and 1·79, respectively.

Rb–Sr analyses were carried out on ~100 mg of whole-rock powders and mineral separates (Table 3). Except for aliquot >0·50 mm (2d), which was wet ground like the 0·16–0·25 mm fraction and then sieved again to recover the <0·10 mm (2d-1) and >0·25 mm (2d-2) grain fractions, white mica fractions were the same as those used for ^{40}Ar–^{39}Ar analyses. Samples were dissolved into Savillex screw-top beakers using a mixture of HF and HNO_3. One aliquot was spiked using a mixed ^{87}Rb–^{84}Sr spike solution. Rb and Sr were separated using standard separation techniques. Total Rb and Sr procedural blanks were lower than 1 and 0·25 ng, respectively. Data were not corrected for blanks because of the very slight effect on the calculated ages. For example, applying blank correction on the phengite fraction with the lowest Sr content [i.e. phengite (2d-2) of sample CM1; Table 3] and assuming a pessimistic blank correction as high as 0·5 ng of Sr with an $^{87}Sr/^{86}Sr$ ratio of 0·707, the $^{87}Sr/^{86}Sr$ of phengite increases by 0·4% and the $^{87}Rb/^{86}Sr$ by 1·3%. These factors produce a decrease in the calculated calcite–phengite age of 0·2 Ma. Blank correction on Rb data for calcite in sample CM1 has an undetectable effect on the calculated two-point (calcite–phengite) isochron ages. An uncertainty of 1% was assigned to the Rb/Sr ratio on the basis of replicate analyses on natural samples. An error of 5% was instead used for calcite. At the time of data collection the NIST SRM 987 yielded an average of 0·710240 ± 0·000016 (2σ, n = 16), which was assumed to be the minimum uncertainty in isochron calculations. Isochrons were calculated by the Isoplot/Ex program, v. 3.00 (Ludwig, 2003).